



TOPICAL REVIEW • OPEN ACCESS

## Optoelectronic oscillator for 5G wireless networks and beyond

To cite this article: Fang Zou *et al* 2021 *J. Phys. D: Appl. Phys.* **54** 423002

View the [article online](#) for updates and enhancements.

 <p><b>The Electrochemical Society</b> <small>Advancing solid state &amp; electrochemical science &amp; technology</small> 2021 Virtual Education</p> <p><b>Fundamentals of Electrochemistry:</b> Basic Theory and Kinetic Methods Instructed by: <b>Dr. James Noël</b> Sun, Sept 19 &amp; Mon, Sept 20 at 12h–15h ET</p> <p><b>Register early and save!</b></p>	
---	--

## Topical Review

# Optoelectronic oscillator for 5G wireless networks and beyond

Fang Zou<sup>2,7</sup> , Lei Zou<sup>3,7</sup>, Bo Yang<sup>4,\*</sup> , Qian Ma<sup>5</sup>, Xihua Zou<sup>1</sup>, Jim Zou<sup>6</sup>, Siming Chen<sup>3</sup>, Dusan Milosevic<sup>2</sup>, Zizheng Cao<sup>2,\*</sup>  and Huiyun Liu<sup>3</sup> 

<sup>1</sup> Center for Information Photonics and Communications School of Information Science and Technology, Southwest Jiaotong University, and CSNMT International Cooperation Research Center of China, Chengdu 611756, People's Republic of China

<sup>2</sup> Institute for Photonic Integration, Eindhoven University of Technology, Eindhoven 5600 MB, The Netherlands

<sup>3</sup> Department of Electronic and Electrical Engineering, University College London, London WC1E 6BT, United Kingdom

<sup>4</sup> School of Communication Engineering, Hangzhou Dianzi University, Xiasha, Hangzhou, 310027, People's Republic of China

<sup>5</sup> Extreme Waves LLC, 12348 Highbluff Dr STE 100, San Diego, CA 92130, United States of America

<sup>6</sup> ADVA Optical Networking SE, 98617 Meiningen, Germany

E-mail: [yangbozju@hdu.edu.cn](mailto:yangbozju@hdu.edu.cn) and [z.cao@tue.nl](mailto:z.cao@tue.nl)

Received 25 January 2021, revised 23 May 2021

Accepted for publication 13 July 2021

Published 3 August 2021



## Abstract

With the development of 5G wireless network and beyond, the wireless carrier frequency will definitely reach millimeter-wave (mm-wave) and even terahertz (THz). As one of the key elements in wireless networks, the local oscillator (LO) needs to operate at mm-wave and THz band with lower phase noise, which becomes a major challenge for commercial LOs. In this article, we investigate the recent developments of the electronic integrated circuit (EIC) oscillator and the optoelectronic oscillator (OEO), and especially investigate the prospect of OEO serving as a qualified LO in the 5G wireless network and beyond. Both the EIC oscillators and OEOs are investigated, including their basic theories of operation, representative techniques and some milestones in applications. Then, we compare the performances between the EIC oscillators and the OEOs in terms of frequency accuracy, phase noise, power consumption and cost. After describing the specific requirements of LO based on the standard of 5G and 6G wireless communication systems, we introduce an injection-locked OEO architecture which can be implemented to distribute and synchronize LOs. The OEO has better phase noise performance at high frequency, which is greatly desired for LO in 5G wireless network and beyond. Besides, the OEO provides an easy and low-loss method to distribute and synchronize mm-wave and THz LOs. Thanks to photonic integrated circuit development, the power consumption and cost

<sup>7</sup> These authors contribute equally to this work.

\* Authors to whom any correspondence should be addressed.



Original content from this work may be used under the terms of the [Creative Commons Attribution 4.0 licence](https://creativecommons.org/licenses/by/4.0/). Any further distribution of this work must maintain attribution to the author(s) and the title of the work, journal citation and DOI.

of OEO reduce gradually. It is foreseeable that the integrated OEO with lower cost may have a promising prospect in the 5G wireless network and beyond.

**Keywords:** 5G, local oscillator, optoelectronic oscillator

(Some figures may appear in color only in the online journal)

## Preface

Compared to the previous generation of mobile communication, the 5th-generation new radio (5G NR) standardized by the 3rd generation partnership project (3GPP) presents some improvements, including enhanced mobile broadband, ultra-reliable and low latency communications, and massive machine-type communication [1–5]. To achieve these goals, 3GPP has introduced a network architecture [4], with a new physical layer design that supports small-cell architectures, very high carrier frequencies, and a series of new techniques such as massive multiple-input and multiple-output (MIMO), and beamforming features [5]. Furthermore, the beyond 5G (B5G) and the 6th-generation (6G) are researched in recent years, and they are expected to out-perform 5G in regard of throughput by a factor of 10–100. Although the needs and indicators of 6G are not defined yet, it is foreseeable that some auxiliary technologies in 5G are necessary to be compatible in the 6G era [6, 7]. Beyond that, the carrier frequency will reach millimeter-wave (mm-wave) and terahertz (THz). In addition, more efficient modulation methods will be explored in the 6G, and more antennas will be used in the base station (BS) due to the small-cell architecture and the massive MIMO in 6G.

As one of the key elements in the wireless network, the local oscillator (LO) often serves as a reference for the carrier signal to up- and down-convert the output and incoming data. Therefore, the LO also needs to meet some new requirements. Recently, some mature electronic integrated circuit (EIC) oscillators have been implemented in the 5G FR1 and a lot of efforts are devoted to research the LO in 5G FR2 and B5G by using the mm-wave and THz EIC oscillators [8–10]. Besides, a fiber-compatible and high-quality LO based on the optoelectronic oscillator (OEO) is regarded as a potential technology in the 5G wireless network and beyond.

The new architectures and requirements of the 5G wireless network and beyond provide an opportunity to utilize the fiber-based fronthaul. On the one hand, the optical fronthaul has the characteristics of broadband, ultra-low loss and low latency [11, 12]. On the other hand, given the 5G and B5G small-cell architecture, only the optical fronthaul is able to accommodate the tremendously increased number of access points. The massive implementation of optical fronthaul is necessary for implementing the OEOs [13]. Since the optical fronthaul consists of optical and electronic parts, it enables the OEO loop without extra configurations. Besides, the enhanced mobile broadband and complex modulated format will be used in the 5G wireless network and beyond. Hence, a mm-wave or THz LO with ultra-low phase noise is expected to reduce the error vector measurement (EVM) caused by the phase-noise jitter. Thanks to the high- $Q$  value providing by long fiber, the

OEO realizes an ultra-low phase noise and the phase noise is independent of oscillating frequency. The OEO can easily meet the requirements of phase noise when it serves as LO in the 5G wireless network and beyond. More importantly, the increased number of the access point needs a large number of LOs to generate synchronized carrier components (CCs). For example, the CCs in the MIMO and the coordinated multiple points transmission/reception (CoMP) must be synchronized following the 3GPP standard [1, 14]. The OEO provides an easy and economical method for distributing and synchronizing CCs in the access points [15, 16]. Moreover, the synchronization of OEOs is independent of the GPS, which is suitable for the private network in 5G wireless network and beyond. Therefore, we introduce the OEO for 5G wireless network and beyond in this article.

The diverse applications of OEO have been inspired and attached much attention in recent years. Many reviewed articles introduce the OEO applications in terms of sensing, microwave signal generation for radar, chaos communications and optoelectronic machine learning [17–20]. In this article, we review the OEO in a new aspect and discuss the prospect that OEOs serve as both the single-point LO and LOs networks in the 5G wireless network and beyond.

The outline of the paper is shown in figure 1. Section 1 is devoted to the LO and the new requirements for 5G and beyond wireless network. The EIC oscillator, OEO and integrated OEO are reviewed in sections 2–4. We compare the performances of the EIC oscillator and OEO in section 5. In section 6, some specific and new requirements of 5G and key performance indicators (KPIs) of 6G are reviewed, where we discuss the criteria of the LO according to the standards of 5G and beyond. In section 7, we propose an OEO network that satisfies distribution and synchronization of LOs in 5G wireless network and beyond. Researched prospect for OEO-based LOs distributing network is discussed in the last section following by the conclusion. In conclusion, we believe the distributing LOs network based on the integrated OEO has a promising prospect in the 5G wireless network and beyond.

## 1. LO for 5G and beyond wireless network

### 1.1. LO

A natural phenomenon exhibiting a repetitive variation of displacement about a center point or between two states in time, is defined as oscillation. The oscillation occurs in mechanical systems and dynamic systems in virtually every field of human experience, such as occurring in the human heart, the business cycle, the population cycle, and the geothermal geysers [21]. Phenomenon-based oscillators have been designed and

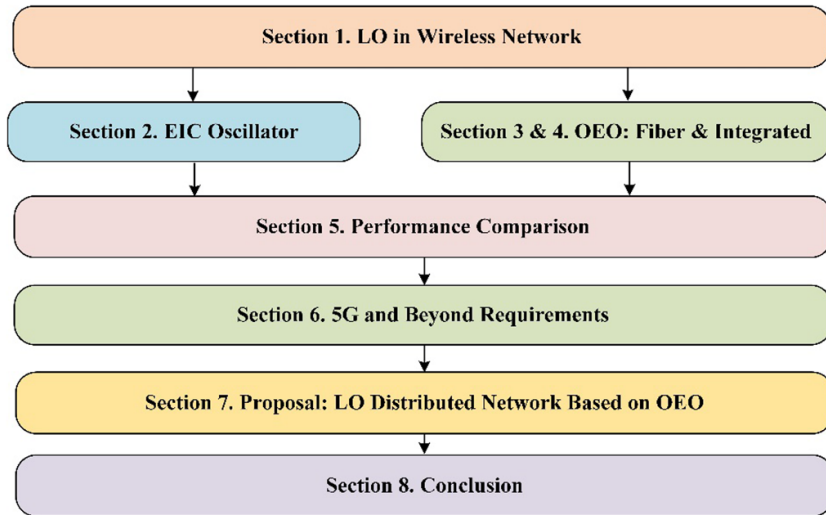


**Figure 1.** The outline of the review.

are perhaps the most widely used devices. For example, a variety of mechanical (e.g. the pendulum), electromagnetic and atomic oscillators provide a diverse range in the approximation to the realization of the ideal harmonic oscillator [22–29].

In the digital and information era, a widely used type of oscillator is the electronic oscillator. It generates a periodic, oscillating electronic signal, typically a sine wave or a square wave by converting the direct current (DC) from a power supply [30]. The electronic oscillator originates from Thomson in 1892, who placed an inductance–capacitance (LC) tuned circuit in parallel with an electric arc [31]. Then, a vacuum tube oscillator is invented in 1912 by using electrical feedback. Three years later, the Hartley oscillator with two coils forming a shared inductance was invented. By tuning the circuit consisting of capacitors and inductors, the oscillating frequency can be adjusted. It is the 1st LC oscillator and leads to the boom of electronic oscillating technology in the following century [32–34]. In the 20th century, thanks to the evolution of integrated circuits following Moore’s law [35, 36], EIC oscillators have achieved dramatic performances in terms of oscillating frequency, levels of integration, stability, phase noise, and power consumption [37–39]. The EIC oscillators are widely used in almost every information and communication system, such as the central processing unit of the computer [40], radar system [41–43], and sensor system [44–46]. Specifically, the EIC oscillators are always used in the super-heterodyne receiver, which is the most common type of radio receiver circuit which is well known in the modern wireless communication systems as the LO.

LO often serves as a reference for the carrier signal to up-convert and down-convert the output and incoming data, respectively. When the radio signal with data is received and demodulated, recovering and synchronizing the carrier are always required. The LO should be a clean and stable source so that the transceiver can well synchronize and recognize the carrier. The phase noise of the LO should be low enough to ensure a good signal-to-noise ratio (SNR). As the LO is indispensable in the transceiver, improving the performances of LO is an important research topic in the 5G and beyond wireless

network. For example, the phase noise of the LO is a random fluctuation causing detection error of the received signal spectrum. Also, the phase noise of LO destroys the orthogonality of the subcarriers in orthogonal frequency division multiplexing systems and degrades the performance by producing intercarrier interference [47–53].

## 1.2. New requirements on the LO for 5G and beyond

To support more complex services in 5G and beyond, the broader bandwidth (BW) and more efficient modulated formats are necessary [1–5]. Hence, LOs with high frequency and outstanding performances are crucial for the 5G and beyond wireless network. Some new requirements on the LO for 5G and beyond are summarized in the following.

Firstly, an ultra-stable LO in the frequency band of mm-wave or THz is required. The frequency error in the transceivers is mainly attributed to the frequency accuracy of the LOs, and the environment factors (e.g. temperature) may also deviate the carrier frequencies. Besides, the higher carrier frequency poses challenges in synchronizing the CCs and recovering the baseband signal since mm-wave and THz band exhibit more loss and nonlinearity. To solve these problems, a more accurate and stable oscillator with a high frequency is necessary.

Secondly, high-order modulated formats such as 128/256 QAM can improve the spectrum efficiency and realize an ultra-high bit rate [4]. To realize the complex modulated formats, the SNR and the EVMs are critical in the transceiver. For simplicity, the EVM is an integration of phase noise beyond tracking BW and inside channel BW. Therefore, the phase noise of the LO affects the performance of the transceiver directly.

Thirdly, small cells will also play an important role in 5G and beyond wireless network since the small cells are used to reduce loss of the wireless link and increase data rates. When using small-cell architecture and massive MIMO technology, a large number of LOs are needed in the wireless network with the increasing of the transceiver. From the perspective of the frequency synchronization and the cost reduction, generating

CCs in a center baseband unit (BBU) pool and distributing it to remote radio units (RRUs) may arise as a feasible option [5].

## 2. Description of EIC circuit oscillator

There are some new requirements to realize the new applications in 5G wireless network and beyond, including higher carrier frequency, broader BW, and more efficient modulated formats. Thus, the LO with high frequency and outstanding performance is necessary for the 5G and beyond wireless network, as discussed in section 1. This section introduces the EIC oscillator in terms of the basic concept, prototyped topology, and some key technologies. Besides, we review some EIC oscillators based on submicron CMOS technologies, which can be implemented in the 5G and beyond wireless communication network.

### 2.1. Integrated circuit oscillator

Based on a feedback system, a simple oscillator is used to generate a periodic signal without any input. In the feedback system, if the amplifier experiences so much phase shift at high frequencies that the overall feedback becomes positive, the feedback system would be a self-starting oscillator. More accurately, the feedback system should satisfy that the gain exceeds unit and the phase shifts  $180^\circ$  which are known as the Barkhausen criteria. In COMS technologies, the topology of the oscillator is typically implemented as the ring oscillator or the LC oscillator [54, 55].

According to Barkhausen criteria, the ring oscillator consists of three or more stages (must be odd) amplifiers, as shown in figure 2(a). And beyond that, the differential implementations also can realize ring oscillators by using even number stages. Since the monolithic inductors are widely fabricated by CMOS technologies in the last 20 years, the passive resonant circuit based on LC is one of the most popular topologies in radio-frequency integrated circuits. The typical LC oscillator consists of the parallel between an inductor and a capacitor. And a trans-conductor serves as an active element to balance the tank's unavoidable losses in the LC oscillator, as shown in figure 2(b). Such an LC oscillator ideally oscillates at the tank resonant angular frequency,  $\omega_0 = 1/\sqrt{LC}$ . Based on the basic prototyped topologies, some key technologies have been researched. For example, the voltage-control oscillating (VCO) and the phase-locked loop (PLL) are used to realize RF signal generation with high frequency and quality.

### 2.2. VCO and PLL

The tunable frequency is required in many applications of oscillators. Specifically, the output frequency is a function of the controlled voltage. For example, the oscillating frequency of LC topology is equal to  $f_{osc} = 1/2\pi\sqrt{LC}$ . The oscillating frequency can be adjusted by tuning the inductor or capacitor in the LC topology. Since tuning the value of inductors is difficult in the EIC, the tank capacitance is usually used to tune the oscillating frequency.

According to the 5G standard released by 3GPP, the mm-wave bands include 24.25–29.5 GHz and 37–40 GHz and

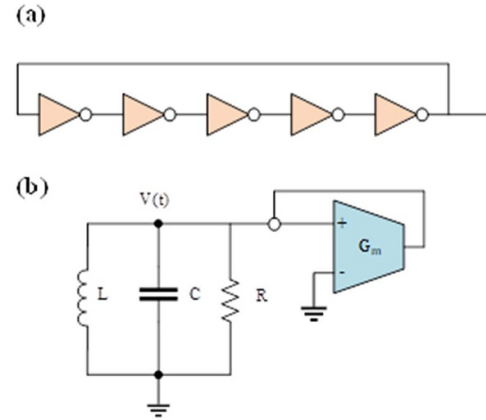


**Figure 2.** The tank of the oscillators: (a) five-stages ring oscillator and (b) LC oscillator with a trans-conductor.

**Table 1.** Reviews of mm-wave signal generation.

Freq (GHz)	PN at 1 MHz (dBc Hz <sup>-1</sup> )	Area (mm <sup>2</sup> )	Tech	Pow (mW)	Ref
23.75	−119.5	0.423	130 nm BiC-MOS (VCO)	122	[56]
25.48	−115.27	0.08	65 nm COMS (VCO)	22	[57]
20.77	−106.6	—	65 nm COMS (VCO)	12.65	[58]
25.4	−112.8	0.24	65 nm COMS (iSS-PLL)	10.2	[59]
35.84	−94.9	1.368	45 nm COMS (RS PLL)	20.6	[60]
28 or 39	−122	0.8	120 nm BiC-MOS (VCO)	103 ~ 188	[61]

Freq: frequency, PN: phase noise, Tech: technology, Ref: reference, Pow: power.

the flexible intermediate-frequency (IF) range is 3–6 GHz. Therefore, LO needs to provide a very wide tunable range for the 5G wireless network. To accelerate the utilization of the 5G in mm-wave, some VCOs have been proposed and demonstrated, as displayed in table 1. In [56], Quadrelli *et al* proposed a Colpitts VCOs tank based on SiGe BiCMOS technology. The four oscillators operate from 18.2 to 21.8 GHz, 20.9 to 24.7 GHz, 23.4 to 27.8 GHz and 25.4 to 29.3 GHz, respectively. The phase noises are from  $-119.5$  dBc Hz<sup>-1</sup> to  $-116.5$  dBc Hz<sup>-1</sup> at 1 MHz offset frequency for the tunable frequencies from 18.2 to 29.3 GHz. In [57], Guo *et al* design a multi-resonator RLCM (i.e. resistor–inductor–capacitor–mutual-inductance) tank VCOs to reshape the VCO phase noise impulse sensitivity function. The VCO is prototyped



in 65 nm COMS technology and it generates an mm-wave signal from 25.5 to 29.9 GHz with the phase noise of  $-115.27$  dBc Hz $^{-1}$  (for 25.5 GHz) and  $-112.31$  dBc Hz $^{-1}$  (for 29.9 GHz) at the 1 MHz offset frequency. In addition, Lightbody *et al* proposed a VCO topology that leverages a transformer to magnetically couple the varactor to the core instead of connecting a varactor to the oscillator core directly [58]. The prototype VCO is fabricated by 65 nm CMOS and its tunable frequency range is from 20.77 to 28.02 GHz, while the phase noise is  $-106.6$  dBc Hz $^{-1}$  at 1 MHz offset frequency for 26.45 GHz mm-wave signal.

In addition to the VCO, the PLL is another key technology for improving the quality of LO in the 5G wireless network. PLL is a feedback system that compares the output phase with the input phase to keep the phase-matched. Typically, a PLL consists of a phase detector, a VCO, and a low-passband filter. By controlling the voltage of the oscillator, the jitters in the oscillator, such as input jitter and VCO-produced jitter, can be suppressed and locked to a referenced low-noise crystal oscillator, thereby improving the frequency accuracy and synchronizing with the reference. Besides, the PLL is used for frequency multiplication of VCO as well. To support massive applications in 5G communication, the LO needs to realize high stability (or frequency accuracy) and ultra-low phase noise.

Some mm-wave PLLs have been proposed by using different architectures to improve the frequency accuracy of LO. Yang *et al* reported an isolated-sub-sampling PLL (iSS-PLL) dissipating only 10.2 mW at 26.4 GHz. When it is locked to a 103 MHz reference, a low integrated jitter (71 fs rms) is achieved and the compromising spur is  $-63$  dB [59]. The oscillator generates a mm-wave signal in which the tunable range is from 25.4 GHz to 29.5 GHz and the restored in-band phase noise is  $-112.8$  dBc Hz $^{-1}$  at the offset frequency of 1 MHz when the frequency is 26.368 GHz. In [60], Liao *et al* proposed an mm-wave synthesizer by using robust locking reference-sampling PLL and wide-range injection-locked VCO. The synthesizer is prototyped in 45 nm partially depleted silicon on insulator (SOI) CMOS technology. The 1st stage of 9 GHz RSPLL achieves a 144 fs integrated jitter with 7.2 mW power consumption and the overall mm-wave synthesizer achieves a tunable range of 33.6–36 GHz with a phase noise of  $-94.9$  dBc Hz $^{-1}$  at 1 MHz offset frequency for 35.84 GHz. In [61], a class-C type transformer-coupled VCO is combined with type II charge-pumped-based PLL based on 0.12  $\mu$ m SiGe technology. This proposal generates an mm-wave signal whose frequencies are 20–24 GHz and 30–36 GHz by multiplying the fundamental frequency of 10–12 GHz. The phase noise is  $-122$  dBc Hz $^{-1}$  at the offset frequency of 1 MHz for the fundamental frequency.

### 2.3. THz oscillator (6G)

With the commercial application of the 5G, the research projects about the 6G wireless communication system have been launched. In the future, the 6G decidedly requires a higher frequency for carrying extra-high-speed data. THz technology seems a potential technology to solve the limitation of BW in

**Table 2.** Reviews of THz signal generation.

Freq (GHz)	PN at 1 MHz (dBc Hz $^{-1}$ )	Area (mm $^2$ )	Tech	Pow (mW)	Ref
229	$-85.8$	0.21	65 nm COMS	195	[62]
213	$-93.4$	0.0675	65 nm COMS	11.5	[63]
275	$-81.2$	0.022	130 nm SiGe	42.3	[64]

Freq: frequency, PN: phase noise, Tech: technology, Ref: reference, Pow: power.

6G. Some fully integrated implementation of THz systems in low-cost and reliable silicon technologies have been explored in past years. We review these outstanding proposals in the following and their performances are listed in table 2. In [62], Jalili and Momeni presented a wideband harmonic VCO with large output power by using a coupled standing wave oscillator. The prototype chip implemented in a 65 nm CMOS process covers a 219–238 GHz frequency band with the output power of 3.4 dBm, while the minimum measured phase noise is  $-105.8$  dBc Hz $^{-1}$  at 10 MHz offset frequency. Furthermore, Wang *et al* reported an approach to design compact high-efficiency THz fundamental oscillators and it can be operated above half of the maximum frequency of the active device [63]. A 213 GHz signal-ended and differential fundamental oscillator was fabricated by 65 nm CMOS technology. The phase noise was measured as  $-93.4$  dBc Hz $^{-1}$  at 1 MHz offset. In [64], a new design of harmonic VCO was proposed and fabricated by the 130 nm SiGe processing. Such harmonic VCO generates the THz signals with the tunable frequency from 270.3 GHz to 279.3 GHz, while the phase noise is  $-81.2$  dBc Hz $^{-1}$  at 1 MHz offset frequency for 275 GHz.

### 3. Description of the OEO on fiber

The researchers pursue an energy storage element with the high  $Q$ -value and the ultra-low transmitted loss to realize the pure and stable spectrum when exploring the electronic oscillator. But it is hard to configure a high- $Q$  value in the EIC oscillator because the intrinsic loss would deteriorate the performance of power communication. In 1994, the OEO was proposed for the first time by Yao and Maleki, which converts the continuous light wave into stable and pure microwave signals [29]. Because the commercial fiber has an ultra-low loss, i.e. 0.2 dB km $^{-1}$  for the 1550 nm wavelength, a fiber with the length of kilometers serves as an energy-storage element to realize a high- $Q$  value for the OEO system. Therefore, an oscillator with ultra-low phase and stable spectrum is enabled by using the OEO system.

Typically, an OEO system consists of a tunable laser source, an electro-optical modulator (EOM), and an optical delay line, a photodetector (PD), an electrical amplifier (EA), and an electrical band-pass filter (EBPF). A Mach-Zender modulator (MZM) usually serves as the EOM and a single-mode fiber (SMF) serves as the optical delay line. The light emitted from

a tunable laser source is transmitted through the SMF after modulated by the MZM. Then, the modulated light is detected at the PD, where the light converts to an RF signal by the optical envelope detection. In the RF section, an EA and an EBPF are necessary for providing enough gain and selecting the oscillating mode. Only the loop gain exceeds the total loss at a certain frequency while its phase increases  $2\pi$  in each circulation, could the selected mode steadily oscillate. Under these criteria, OEO generates a RF signal with high frequency and ultra-low phase noise. In this section, we review the OEO technology in terms of the theoretical model, the application and some milestones in application, representatively.

### 3.1. Modeling for OEO

The first theoretical model of the OEO was proposed by Yao–Maleki in 1996 [65]. Based on the quasi-linear theory, the overall relationship between the output of the amplifier and the input of the EOM is analyzed. By using the regenerative-feedback approach, this model analyzes the final steady-state spectra of OEO after thousands of oscillations. Furthermore, in order to analyze the dynamical effects from the start-up to the stable oscillation, Levy *et al* introduce a slow variation on the amplitude envelope. Thus a new and comprehensive model is proposed for single-loop OEO [66]. Beyond the physical effects in the Yao–Maleki model, this model as well as includes some dynamical effects of OEO, such as the fast response time of the modulator, the ability of the OEO to oscillate in several modes and signal fluctuations induced by the input noise. Except for the quasi-linear theory, Chembo *et al* proposed a nonlinear dynamic approach to study the signal dynamics in OEO [67]. Using the delay-differential equation (DDE), the model could analyze the interaction between the delay and the intrinsic nonlinearity resulting in unsuspected bifurcation-induced instability. However, this model assumes that the mode space is smaller than the BW of the filter and signal variation is small. In other words, it is not a general model for the OEO system. In this review, we take the comprehensive model proposed by Levy *et al* as an example to analyze the physical effects, including both steady state and dynamic processing in oscillating.

The schematic of the OEO is shown in figure 3. To analyze the relationship between the input signal of the EOM and the output of the EA, we assume the input signal is  $V_{in}(t, T)$  and the output signal is  $V_{out}(t, T)$ . Because the quality factor of the EBPF is extremely high, the  $V_{in}(t, T)$  can be approximated as a sinusoidal wave with an angular frequency  $\omega_c$ , a time dependent phase  $\phi(T)$  and a time dependent amplitude  $|\alpha_{in}^{mod}(T)|$ . We can express it as:

$$\begin{aligned} V_{in}(t, T) &= |\alpha_{in}^{mod}(T)| \cos[\omega_c t + \phi(T)] \\ &= \frac{1}{2} \alpha_{in}^{mod}(T) \exp(-i\omega_c t) + cc \end{aligned} \quad (1)$$

where  $\alpha_{in}^{mod}(T) = |\alpha_{in}^{mod}(T)| \exp[-i\phi(T)]$  is the complex envelope of the input voltage  $V_{in}(t, T)$ . It is noticed that the expression of the input voltage includes two kinds of the time scale.

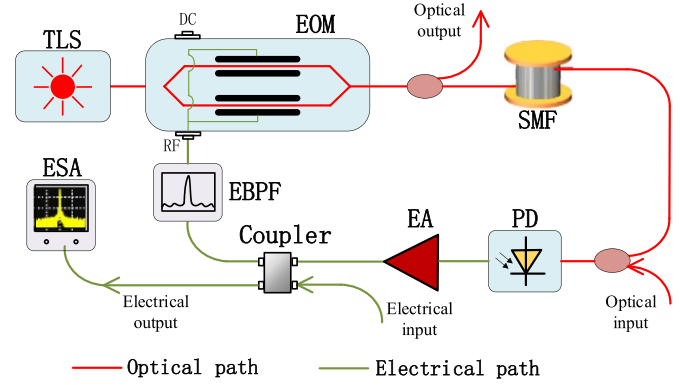


**Figure 3.** Schematic of a classical OEO system. (TLS, tunable laser source. EOM, electro-optical modulator. SMF, single mode fiber. PD, photodetector. EA, electrical amplifier. EBPF, electrical band-pass filter. ESA, electrical spectrum analyser).

Specifically, a slow time scale  $T$  is determined by the round-trip time ( $1\text{--}10\ \mu\text{s}$ ) and a fast time scale  $t$  is order of the periods of sinusoidal wave ( $10\text{--}100\ \text{ps}$ ). In addition, there is another time scale to describe the optical signal, but it can be ignored in this model. The output optical signal is determined by the  $V_{in}(t, T)$  according to the nonlinear response of the EOM. Then the optical signal is converted to an RF signal and amplified to output electrical signal  $V_{out}(t, T)$ , which can be written as:

$$V_{out}(t, T) = V_{ph}(1 - \eta \sin\{\pi[V_{in}(t, T)/V_{\pi} + V_B/V_{\pi}]\}) \quad (2)$$

where  $V_{ph} = I_{ph}RG_A$  is the PD voltage,  $I_{ph} = \rho\alpha P_0/2$  is the detected photocurrents at the PD,  $R$  is resistor,  $G_A$  is the amplified coefficient.  $V_{\pi}$  and  $V_B$  is the half-wave voltage and the DC bias voltage of the modulator.  $\eta$  is defined as the extinction ratio of the modulator,  $(1 + \eta)/(1 - \eta)$ . Combining the equations (1) and (2), we use the Jacobi–Anger expansion to describe their relationship:

$$\begin{aligned} V_{out}(t, T) &= DC + HH + cc - \eta V_{ph} J_1(\pi |\alpha_{in}^{mod}(T)| / V_{\pi}) \\ &\quad \times \exp[-i\omega_c t + i\phi(T)] \end{aligned} \quad (3)$$

where  $J_1$  is the 1st order of Bessel's function. Because the high-order harmonics (HH) and the DC are blocked by the EBPF and DC-block of PD, we may neglect them by using the quasi-linear theory when rejected back to the MZM, while the nonlinear effects of high-order modes on the amplifier saturation is similarly neglected due to the quasi-linear theory.

Using quasi-linear theory approximation, only the 1st-order mode at the carrier angular frequency of  $\omega_c$  would propagate within the cavity. Hence, the complex envelop of the EA output voltage can be written as:

$$\alpha_{out}^{amp}(T) = -2\eta V_{ph} J_1(\pi |\alpha_{in}^{mod}(T)| / V_{\pi}) \exp[i\phi(T)]. \quad (4)$$

It is clear that the amplitude  $\alpha(T)$  and phase  $\phi(T)$  are variable on a slow time scale. We assume the response EBPF is Lorentzian shape. After the EBPF, the filter output  $\alpha_{out}^{fil}(T)$  can be described by the Fourier coefficient of filter input  $\tilde{\alpha}_{in}^{fil}(f_k)$  and filter impulse response  $F(f_k + f_c)$ ,

$$\begin{aligned}\alpha_{\text{out}}^{\text{fil}}(T) &= \text{IFFT}(\tilde{\alpha}_{\text{out}}^{\text{fil}}(f_k)) = \text{IFFT}(\tilde{\alpha}_{\text{in}}^{\text{fil}}(f_k) \times F(f_k + f_c)) \\ &= \text{IFFT}\left(\tilde{\alpha}_{\text{in}}^{\text{fil}}(f_k) \times \frac{i\Gamma/2}{f_k + f_c - f_0 - i\Gamma/2}\right)\end{aligned}\quad (5)$$

where  $\tilde{\alpha}_{\text{in}}^{\text{fil}}(f_k)$  is the Fourier transform of  $\alpha_{\text{out}}^{\text{amp}}(T)$ ,  $f_k$  is the offset frequency with respect of the chosen carrier frequency  $f_c$ ,  $f_0$  is the central frequency of the filter and  $\Gamma$  is the full width at half-maximum of filter transmission spectrum.

The complex amplitude of the signal inside the OEO on a round trip is calculated, then it would be iterated thousands of times to simulate the oscillation. The complex amplitude  $\alpha^l(T)$  is defined as the interval of  $\alpha_{\text{in}}^{\text{fil}}(T)$  in  $(l-1)\tau \leq T < l\tau$ , where the  $l$  is the number of round trips and  $\tau = n_{\text{eff}}L/c$  is the round-trip time of the OEO cavity. The next round trip  $\alpha^{l+1}(T)$  is equal to the valid convolution between the amplitudes of the former adjacent two round trips and the filter impulse response. Then, the complex amplitude is fed back to the modulator, and calculate the response of EOM and PD within the next round trip. The noises including the thermal noise of amplifier, the shot noise of PD and the intensity noise of laser are added in the input of amplifier. We can approximate the total noises in the OEO as a white Gaussian noise with a single-sideband power spectral density of  $\rho_n$ .

After thousands of iterations  $T_0 = N\tau$ , we can get a steady-state oscillation. To analyze the performance of the OEO system,  $\alpha_{M\tau}(T)$  is defined as the voltage amplitude for the time range from  $T_0$  to  $T_0 + M\tau$  and its discrete Fourier transform can be written as:

$$\tilde{\alpha}_{M\tau}(f) = F_{M\tau}[\alpha(T)] = \frac{1}{M\tau} \int_0^{M\tau} \alpha_{M\tau}(T + T_0) \exp(2\pi ifT) dT. \quad (6)$$

In the theoretical model, the RF spectrum is approximately equal to the phase noise spectrum over a wide frequency range in OEO since the amplitude noise is negligible and the phase fluctuation is much smaller than unit [58]. This approximation had been demonstrated in the theoretical simulation and experiment demonstration in former research. We can evaluate the performance of phase noise in the model by:

$$S_{\phi}^{M\tau}(f) \cong S_{\text{RF}}^{M\tau}(f) = \frac{|F_{M\tau}[\alpha(T)]|^2}{2RP_{\text{osc}}\delta f} \quad (7)$$

where  $P_{\text{osc}} = |\tilde{\alpha}(f=0)|^2 / 2R$  is the carrier power.

Base on the single-loop OEO model, other complex theoretical models for simulating different OEO configurations had been developed, such as the multi-loop OEO [68–70], tunable OEO by using microwave filter [71] and coupled OEO (COEO) system [72–74].

### 3.2. OEO for microwave generation

As a representative microwave-photonics device, OEOs have already been implemented in many applications. For instance, the OEOs are used to generate, process, and detect the RF signals [17–20]. Particularly, OEOs achieve excellent phase noise because of the high- $Q$  storage element. The feature

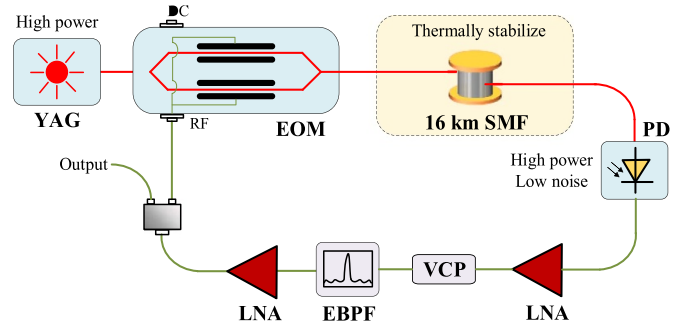


**Figure 4.** Schematic of OEO with ultra-low phase noise. (YAG laser: yttrium aluminum garnet laser, VCP: voltage-controlled phase shifter, LNA: low noise amplifier).

of the ultra-low phase noise makes OEO suitable for LOs for radar and communication systems. In the following, we review some quintessential OEO architectures for RF signal generation, including the single-loop OEO, the multi-loop OEO, the injection-locked OEO, the COEO and the tunable OEO.

**3.2.1. Single-loop OEO.** Single-loop OEO is a conventional architecture that is firstly invented by Yao and Maleki. By optimizing the noise and using a long fiber, some ultra-high-performance units had been realized. Specifically, OEwaves Inc. directed by Maleki proposed a microwave generator based on single-loop OEO with a long fiber delay [72], as shown in figure 4.

Light emitted from a high-power YAG laser is modulated by a lithium niobate MZM. After the MZM, the light is subsequently transmitted in a 16 km long fiber which is placed in a thermally stabilized box to reduce frequency drift. Then the light is detected by a high-power and low-noise PD. In the electrical processing, after a LNA, the microwave signal is sent to a voltage-controlled phase shifter and an EBPF which are used to select the oscillating mode in the oscillation finely. Finally, the microwave signal is amplified by a LNA and fed back to the MZM. Such an oscillator generates a stable 10 GHz signal with a phase noise of  $-163$  dBc  $\text{Hz}^{-1}$  at 6 kHz offset frequency, which is the lowest phase noise for all types of oscillators as far as we know.

**3.2.2. Multi-loop OEO.** For achieving an ultra-high performance OEO, a long fiber delay would be introduced in the oscillating cavity. The oscillating mode space is reciprocal of the length of the cavity. For example, the mode space decreases to 10 kHz when a 5 km length SMF is used. The modes competition would deteriorate the oscillating stability. Thus, an EBPF with a sharp response is necessary if we want to generate a stable RF signal with high spectral purity. Nevertheless, fabricating a high- $Q$  filter at high frequency is difficult and expensive. And the fixed central frequency of the filter also limits the tunability of the OEO system.

To solve this problem, multi-loop OEO seems an effective method [68]. The multi-loop OEOs with different loop lengths are implemented to configure a self-sustained filter-less



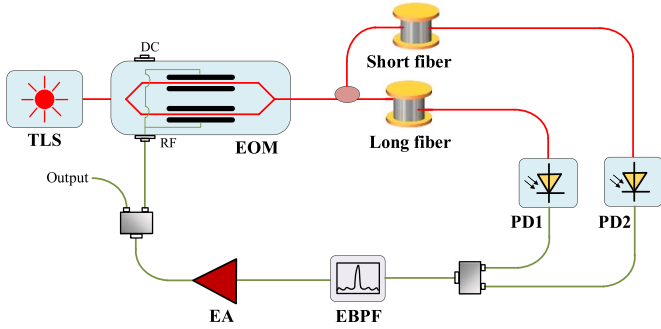


Figure 5. Schematic of multi-loop OEO.

oscillator, as shown in figure 5. The longer loop determines the phase noise of OEOs, and mode space depends on the shorter loop. When some of the oscillating modes generated by each loop are in phase, a stable oscillation can be achieved by the Vernier effect. These oscillating frequency of the modes must satisfy:

$$f_{\text{osc}} = \frac{k}{\tau_1} = \frac{m}{\tau_2} \quad (8)$$

where  $k$  and  $m$  are integers,  $\tau_1$  and  $\tau_2$  are time delays for each loop. Thus, the mode space is enlarged and the side modes can be easily suppressed by using an EBPF. A 30 dB reduction of spurious levels has been demonstrated by using the scheme shown in figure 5. However, the overall  $Q$  is approximately an average of two different length loops. Its phase noise is relatively high, when using same length of fiber in single-loop OEO.

**3.2.3. Injection-locked OEO (IL-OEO).** As aforementioned, we can use the dual-loop OEO to realize stable oscillation without an EBPF. However, the dual-loop OEO sacrifices the high  $Q$  produced by the long fiber. Because the overall  $Q$  is determined by the  $Q$ -values of longer loop and shorter loop, the phase noise would increase compared with the single-loop OEO. To solve this problem and suppress the mode spurs, the IL-OEO is proposed [69, 70]. In the demonstration of IL-OEO, Zhou *et al* use a master OEO with long-loop to injection-lock a short-loop single-mode slave oscillator [69], as shown in figure 6. Because of the frequency pulling effect, the spurious suppression of OEO can be achieved when another signal with a close frequency and enough power is injected. In this proposal, the preliminary phase-noise measurement indicates an approximately 140 dB reduction of the spurious level. Based on the IL-OEO, Okusaga *et al* employed two OEOs that inject and affect each other to mutually injected lock [70], which is known as the dual-loop IL-OEO. The steady-state power fluctuation in either loop achieved both lower phase noise and lower spurs, comparing with the dual-loop OEO. Moreover, the self-injection locked and phase-locked loop (SILPLL) is also used to further reduce the phase noise and time jitter. For example, A. Daryoush's group developed self-forced oscillators by using SILPLL technology [75–77] and realized ultra-low phase noises for the dual-loop OEOs.

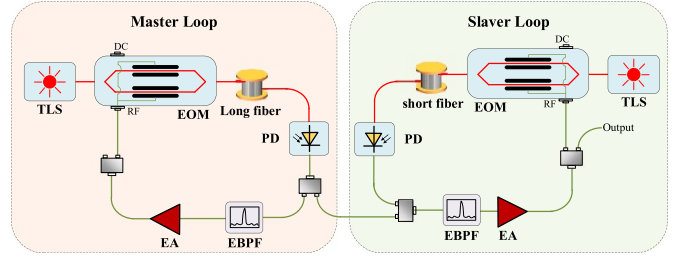


Figure 6. Schematic of dual IL-OEO.

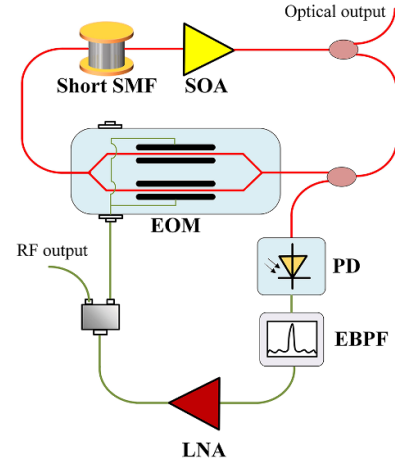


Figure 7. Schematic for COEO.

Such phase noises are  $-125 \text{ dBc Hz}^{-1}$  [75],  $-137 \text{ dBc Hz}^{-1}$  [76] and  $-138 \text{ dBc Hz}^{-1}$  [77] at 10-kHz offset frequency when the oscillating frequency is 10 GHz. Especially, a high-resolution X-Band frequency synthesizer based on SILPLL OEO is reported in [77]. Its associated time jitter (integrating from 300 Hz to 10 MHz) is calculated as 5.17 fs for a 12-GHz carrier by using a custom chirped fiber Bragg grating. The time jitter (or phase jitter) is the key parameter of LO in the communication system which directly affects the EVM of complex modulated format.

The IL-OEO is available in the communication system due to the characteristic of distribution, and we discuss how to implement the IL-OEO architecture in wireless communication and what are the conditions that should be considered in section 7.

**3.2.4. COEO.** In contrast to the OEO, laser oscillation is directly coupled with the electronic oscillation in the COEO configuration. Since the COEO configuration includes a positive optical feedback loop around the high  $Q$  element, the  $Q$  enhancement is multiple the quality factor of the passive storage element, which results in using a compact scheme to realize the same performance. A detailed example of a COEO configuration is shown in figure 7, which consists of an optical loop and an electrical section. In the optical loop, a ring laser is configured by a semiconductor optical amplifier and an MZM around a high- $Q$  element. After detected by a PD, the

microwave signal is amplified and filtered in the RF section, and then fed back to the ring laser via MZM.

A typical COEO configuration is demonstrated in [72]. A fiber with a length of 140 m is used to generate a 10 GHz RF signal with a phase noise of  $-148$  dBc Hz $^{-1}$  at 10 kHz offset frequency. The conventional OEO configuration needs 4 km length fiber to realize the same phase noise. The utilize of shorter fiber in COEO leads to a compact size and low power consumption. Because of a shorter fiber in the oscillating loop, the spur is more easily blocked by the filter to improve spectral purity. Besides, the COEO can also be configured as a mode-locked laser with electronic feedback that generates an optical pulse train in the time domain.

**3.2.5. Tunable OEO.** In addition, tunability is another important research topic in OEO for microwave signal generation. In the conventional OEO system, the oscillating frequency is determined by the central frequency of the EBPF. So, if we want to adjust the oscillating frequency, a tunable EBPF is necessary. However, fabricating a tunable filter with sharp response and broadband in high frequency is difficult and expensive. In order to overcome this defect, some tunable OEOs configurations based on microwave photonic filter have been proposed [78–82].

Representatively, Li and Yao proposed and demonstrated an optically tunable OEO by incorporating a tunable microwave photonic filter [78]. In this proposal, a phase-modulation to intensity-modulation (PM–IM) conversion is implemented by using a phase-shifted fiber Bragg grating. A microwave signal with a frequency tunable range from 3 GHz to 28 GHz is generated, while the phase noise for the 10 GHz microwave signal is  $-102$  dBc Hz $^{-1}$  at 10 kHz offset frequency. In [81], Peng *et al* proposed a tunable microwave signal generator, and it utilizes a dual-loop OEO oscillator based on stimulated Brillouin scattering. By directly tuning the wavelength of the pump laser, a widely tunable range from dc to 60 GHz for the microwave signal generation can be obtained, which is the widest fundamental frequency tunable range as we have known. And its phase noise is  $-148$  dBc Hz $^{-1}$  at 10 kHz offset frequency for 5, 10 and 20 GHz signal.

### 3.3. Performances of OEO system

In summary, comparing with the EIC oscillator for microwave signal generation, OEO generates spectrally pure microwave signals in the high-frequency band. In order to achieve the spurious suppression of side modes and maintain the high- $Q$  factor of the OEO loop, the multi-loop OEOs, the IL-OEOs and the COEOs have been proposed [65–87]. Furthermore, OEO architectures based on optical or microwave photonics filter have been developed to enable wideband tunable microwave signal generation. To clear the development of the OEO for microwave signal generation, we summarized some milestones of the OEO applications and their performances in table 3.

As illustrated in table 3, the microwave signal whose frequency exceeds 90 GHz, or phase noise is  $-163$  dBc Hz $^{-1}$  at 6 kHz offset frequency, or tunable range is from dc to

60 can be realized by using different OEO architectures. More importantly, the OEO system seems to be a potential solution for distributing and synchronizing LO with low transmitted loss in the 5G wireless network and beyond. However, these OEOs based on discrete components are too bulky to implement in the real industry. To meet the requirements of practical applications, such as compact size and low driven power, integrated OEOs come into the insight of the researchers. So, in the next section, we focus on reviewing the developments of the integrated OEOs in recent years.

## 4. Integrated OEO

As aforementioned, the OEOs achieve remarkable development in the past 10 years. However, the bottlenecks of bulk size and power consumption hinder the popularization and industrialization of OEO. Hence, the development of photonic integrated circuit (PIC) has pushed OEO technology to a new level in recent years. To meet the requirements of practical applications, compact size, and low driven power, integrated OEOs are highly demanded. Some important integrated OEOs and their performances are reviewed in this section.

### 4.1. Partially integrated OEO

Firstly, some partially integrated OEO architectures are reported on different PIC platforms [88–99]. In [88], a SOI chip including a high-speed phase modulator, a thermally tunable micro-disk resonator (MDR), and a high-speed PD is fabricated, and the integrated OEO is implemented to generate a tunable microwave signal, as shown in figure 8(a). Based on the PM–IM conversion, a frequency tuning range of 8 GHz is realized, and the phase noise is lower than  $-120$  dBc Hz $^{-1}$  at 1 MHz offset frequency. In addition to the SOI chip, the indium-phosphide (InP) platform is widely used to fabricate active devices, especially laser sources, because InP materials have a direct bandgap. In [89], an integrated OEO with a tuning range from 15 to 20 GHz is generated by integrating two distributed feedback (DFB) lasers on an InP chip, as shown in figure 8(b). With the cross-injection and OEO technology, the phase noise is  $-95$  dBc Hz $^{-1}$  at 100 kHz offset frequency. Moreover, to avoid the RF loss caused by external EOM in conventional OEO systems, an integrated OEO by using the optical injection of a directly modulated laser was demonstrated. In [91], Zhang *et al* proposed an OEO based on an integrated multi-section DFB laser, as shown in figure 8(c). Such compact OEO generates a 20.3 GHz microwave signal with a phase noise of  $-115.3$  dBc Hz $^{-1}$  at 10 kHz offset frequency. Recently, a parity-time symmetric OEO based on an integrated mode-locked laser is reported as a breakthrough for developing next generation OEOs [92]. As shown in figure 8(d), by implementing PT-symmetry, we realized a filter-free OEO with the tunable frequency from 24 to 25 GHz. The phase noise is lower than  $-108$  dBc Hz $^{-1}$  at the 10 kHz offset frequency and the fluctuation of phase noise is about 2 dB within the whole tunable frequency range.

**Table 3.** Milestones and performances of OEO.

Scheme	Freq (GHz)	PN at 10 kHz (dBc Hz <sup>-1</sup> )	Year	Ref
Single loop OEO	9.56	−130	1996	[65]
Multi-loop OEO	10	−140	1998	[68]
COEO	18.2	−85	2000	[74]
IL-OEO	10	>−110 (at 10–100 Hz)	2005	[69]
Single loop OEO	10	−163 (at 6 kHz)	2008	[72]
Dual IL-OEO	10	−134	2011	[70]
Multi-frequency OEOs	3–28	−102	2012	[78]
Multi-loop OEO	DC–60	−100	2015	[71]
SILPLL OEO	10	−125	2015	[75]
SILPLL OEO	10	−137	2016	[76]
COEO	10	−117	2017	[73]
Single-loop OEO	10.833	−120	2017	[86]
Tunable OEO	8.6–15.2	−110.88	2018	[82]
COEO	30	−114.4 (at 1 kHz)	2018	[83]
	90	−104		
Single-loop OEO	12–20	−114	2019	[80]
Phase-locked OEO	X-band	−139	2019	[81]
SILPLL OEO	X-band	−138	2019	[77]
Tunable OEO	0–20	−95	2020	[79]
IL-OEO	10	−117.6	2020	[84]
IL-OEO	94.5	−101	2020	[87]

Freq: frequency, PN: phase noise, Tech: technology, Ref: reference, Pow: power.

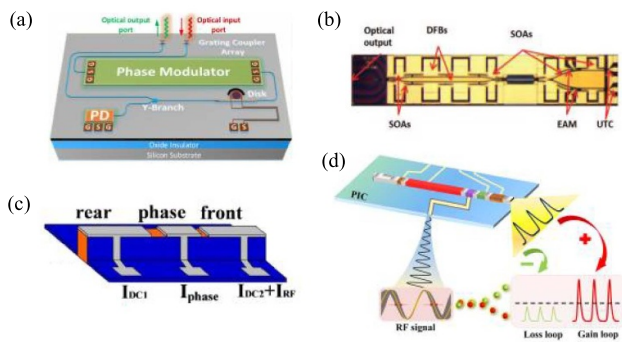


**Figure 8.** The key devices of partially integrated OEO system. (a) A high-speed PM, a thermally tunable MDR, and a high-speed PD (reproduced with permission from [88]. [© Copyright 2018 The Optical Society]), and (b) two DFB lasers on an InP chip (© [2016] IEEE. Reprinted, with permission, from [89]). (c) An integrated multi-section DFB laser. Reproduced from [91]. CC BY 4.0. (d) A parity-time symmetric OEO based on an integrated mode-locked laser. © [2021] IEEE. Reprinted, with permission, from [92].

#### 4.2. Compact OEO module

However, the partially integrated OEOs still use some discrete optical and electrical components. It is hard to further reduce the footprint and cost to meet the requirements of industrialization.

Thus, a lot of efforts were devoted to high-performance microwave oscillators that are not only of miniature size but also have low power consumption. Typically, some compact OEOs are reported in recent years [100–102]. The optical parts of the compact OEOs are integrated and packaged

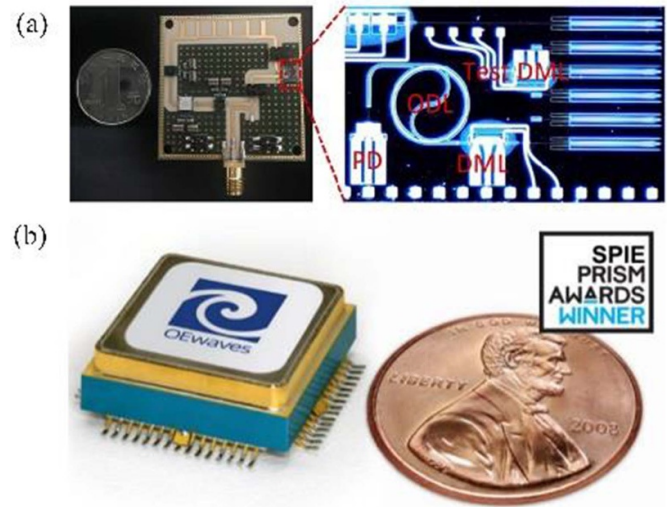


**Figure 9.** The chip of the compact OEOs. (a) A compact OEO that optical parts are integrated and packaged with electrical parts into a miniature module. Reproduced from [100]. CC BY 4.0. (b) Miniature OEO based on a lithium niobate WGMR. Reproduced with permission from [102]. [OEwaves, Pasadena, CA, USA, OE3710 Hi-Q Nano Opto-Electronic Oscillator. [Online]. Available: <https://www.oewaves.com/oe3710>].

with electrical parts into a miniature module. In [100], Tang demonstrated a compact OEO that the optical parts are monolithically integrated on an InP substrate. And the optical and electrical parts are packaged on a print circuit board with the size of  $5 \times 6 \text{ cm}^2$ , as shown in figure 9(a). The oscillating frequencies are 7.30 and 8.87 GHz in different injected currents, and phase noises are  $-92 \text{ dBc Hz}^{-1}$  and  $-93 \text{ dBc Hz}^{-1}$

**Table 4.** Review for integrated OEO.

Partially integrated OEO						
Tech	Freq (GHz)		PN at 10 kHz (dBc Hz <sup>−1</sup> )		Year	Ref
WGMR	8–40		−120		2010	[97]
WGMR on fused SiO <sub>2</sub>	10.7		−90		2010	[95]
MLL on InP	20		−110 (at 10 MHz)		2013	[94]
Disk resonator on SOI	21.7		−90		2013	[96]
DFBL and EAM on InP	15–20		−95 (at 100 kHz)		2016	[89]
Dual-mode laser on InP	37.5–43.59		−94.87		2017	[90]
DML on InP	2–8		−110		2017	[98]
	4–16		−97			
	6–24		−92			
PM and micro-disk resonator on SOI	8		−120 (at 1 MHz)		2018	[88]
DML on InP	2.2–19.5		−110		2018	[93]
Multi-section DEB on InP	20.3		−115.3		2019	[91]
MLL on Inp	24–25		−108		2021	[92]
Multi mode laser and SILPLL OEO on InP	26.4		−92		2021	[99]
Compact OEO module						
Scheme	Freq (GHz)	PN (dBc Hz <sup>−1</sup> )	Size	Pow (W)	Year	Ref
DML	8.87	−92 (at 1 MHz)	5 × 6 cm <sup>2</sup>	—	2018	[100]
WGMR	28–36	−110 (at 10 kHz)	0.06 in <sup>3</sup>	2.5	2010	[101, 102]

Freq: frequency, PN: phase noise, Tech: technology, Ref: reference, Pow: power.

WGMR: whispering gallery mode resonator, MLL: mode-locked laser, DFBL: distributed feedback laser, EAM: electronic absorber modulator, DML: directly modulated laser, PM: phase modulator.

at 1 MHz offset frequency, respectively. In [101], an OEO chip based on a lithium–niobate WGMR has been released by the OEwaves Inc. which is the first commercially used compact OEO module, as shown in figure 9(b). It generates a 28–36 GHz (or higher) microwave signal with a phase noise of  $-110$  dBc Hz<sup>-1</sup> at 10 kHz offset frequency. The size of the OEO chip is 0.06 in<sup>3</sup> and the power consumption is 2.5 W. As a major milestone for OEO, this work exhibits a breakthrough in OEO for microwave generation, and also speeds up real-world applications of OEO [102].

In summary, integrated OEO breaks the bottlenecks of bulky size, high power consumption and environmental perturbation in the traditional OEO system. Some interesting proposals and their performances are listed in table 4.

## 5. Comparing performance between EIC oscillator and OEO

In the previous sections, we review the developments and some applications about the EIC oscillator, discrete OEO and integrated OEO, respectively. In this section, we briefly compare their performances in terms of frequency stability, phase noise, power consumption and cost. The merits and demerits of OEOs and EIC oscillators are also summarized in this section when they serve as a single-point LO device.

### 5.1. Frequency stability

For frequency stability, OEOs and EIC oscillators use the PLL to synchronize the frequency with a referenced crystal.

Therefore, the frequency stability depends on the frequency tolerance of the referenced crystal. Typically, the absolute frequency tolerance of an oven compensated crystal oscillator is 100 ppb with an average frequency from 10 to 100 Hz. After locked by such a reference crystal oscillator, the frequency stability of OEOs or EIC oscillators is sure lower than  $\pm 0.01$  ppm at sub-6G or mm-wave BW. The frequency stability satisfies the 5G or 6G communication system as described in the 3GPP standard.

### 5.2. Phase noise

The OEOs achieve ultra-low phase noise for high oscillating frequency because of the high- $Q$  storage element. Typically, the record phase noise of OEO is  $-163$  dBc Hz<sup>-1</sup> at 6 kHz offset frequency for a 10 GHz microwave signal. Moreover, the phase noise of OEO is independent of the oscillation frequency. Thus, the EVM caused by the phase noise is dramatically optimized when the OEO serves as a LO in mm-wave communication. A statistic for different types of oscillators is illustrated in figure 10. It should be noticed that the offset frequency of 10 kHz is always used to evaluate the phase noise in OEO, while the EIC oscillator usually uses 1 MHz as the offset frequency.

### 5.3. Power consumption and cost

However, there is a long way to go before industrializing OEO in wireless networks due to the high power consumption and high price. Typically, the power consumption of a



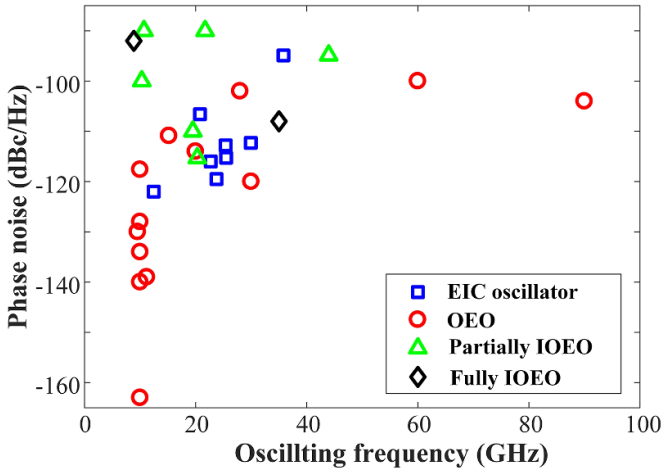


**Figure 10.** Statistics for different type oscillators. (OEO: optoelectronic oscillator, EIC: electronic integrated oscillator, partially IOEO: partially integrated optoelectronic oscillator, fully IOEO: fully integrated optoelectronic oscillator).

discrete OEO is around 10 W and the power consumption of integrated OEO also exceeds 1 W. However, the power consumption of an EIC oscillator is only 10 mW, as illustrated in tables 1 and 2. For massive usage of LOs in remote antennas, low power consumption is exceedingly necessary for future wireless networks. Except for power consumption, the high price of OEO is another weakness. For the discrete OEO scheme, the optical components and high-frequency microwave processing devices are expensive form the lake of industrialization.

In summary, when severing as a single point LO in the 5G and beyond wireless network, OEO and EIC oscillator have the same quality in frequency stability due to the PLL. Since the OEO has a high- $Q$  factor and the phase noise is independent of oscillating frequency, OEO is better than EIC oscillators in the performance of phase noise, especially in the high oscillating frequency. However, the cost and the power consumption of the EIC oscillator are better than the OEO. Fortunately, the PIC technology has developed in three main platforms, including InP, SOI, and silicon nitride ( $\text{Si}_3\text{N}_4$ ) in the past 10 years. A large number of applications by using MPW run within such platforms have been proposed [103, 104]. Maturity in the fabrication process of these materials and their availability through cost-sharing initiatives dramatically reduce the fabrication cost. The PIC technologies provide a promising prospect to industrialize the integrated OEO.

## 6. New requirement of the LO in 5G and beyond wireless network

The performances of EIC oscillator and OEO are introduced in the last section. And we also need to describe the specific criteria of LO, if we want to use the EIC oscillator and OEO in the 5G wireless network and beyond. Therefore, in this section, we introduce the new requirements in the 5G wireless networks, according to the standards released by 3GPP. Furthermore,

**Table 5.** EVM requirement for 5G NR sub-6G in FR1 (410 MHz–7125 MHz).

Modulation scheme	Required EVM
QPSK	17.5%
16 QAM	12.5%
64 QAM	8%
256 QAM	3.5%

based on 5G standards, some KPIs for LO of the 6G wireless network are predicated.

More importantly, the new requirements of wireless networks are focused on the frequency accuracy and EVM of the receiver corresponding to the frequency stability and phase noise of LO. Thus, how to describe the specific requirements of LO to meet the characteristics of 5G and 6G wireless communication systems is discussed in this section.

### 6.1. Characteristics of wireless network

**6.1.1. 5G NR in FR1.** ETSI TS 138 104 provides the requirements for the frequency synchronization applied to 5G networks [4]. The standard states that a wide area BS should use a single-frequency source with an absolute accuracy better than 0.05 ppm for both microwave generation and clocking the time base, while the same source should be used for all carriers of the BS, and the absolute accuracy requirement is relaxed to 0.1 ppm for the medium range and local area BS class. The synchronization requirement of 0.05 ppm has become not only a milestone of mobile-technology-driven requirements for synchronization but also the primary driving force behind recent synchronization studies.

ETSI TS 138 104 also provides the requirements for the EVM levels of each NR carrier for different modulation schemes applied to 5G networks in FR1 [4, 5]. The standard states that the EVM should be better than 17.5% for QPSK and 3.5% for 256 QAM, as listed in table 5.

**6.1.2. 5G NR in FR2.** ETSI TS 138 104 also defines the requirements of frequency synchronization in the mm-wave band. Though the requirement of frequency error in the mm-wave range is also 0.05 ppm for wide-area BS, it is harder for a mm-wave oscillator to achieve the performance.

ETSI TS 138 104 also defines the requirements for the EVM levels of each NR carrier for different modulation schemes in the mm-wave band. The standard states that the EVM should be better than 17.5% for QPSK and 8% for 64 QAM, as listed in table 6.

**6.1.3. 6G KPIs.** Based on the evolution of past generations of wireless communications, the requirements for frequency synchronization and EVM in the 6G era will be higher. Although the technical indicators of 6G have not yet been determined, the use of the mm-wave and THz frequency band is already a recognized trend in order to achieve a higher rate. It means that the frequency error of the mm-wave and THz carrier should be equal to or even better than 0.05 ppm. To

**Table 6.** EVM requirement for 5G NR in FR2 (24 250 MHz–52 600 MHz).

Modulation scheme	Required EVM
QPSK	17.5%
16 QAM	12.5%
64 QAM	8%

**Table 7.** Performance requirements 6G era.

Frequency band	Accuracy	EVM
mm-wave band	$\pm 0.05$ ppm	3.5%
THz band	$\pm 0.05$ ppm	8%

**Table 8.** Frequency error minimum requirement for 5G NR in FR1 (410 MHz–7125 MHz).

BS class	Accuracy
Wide area BS	$\pm 0.05$ ppm
Medium range BS	$\pm 0.1$ ppm
Local area BS	$\pm 0.1$ ppm

**Table 9.** Frequency error minimum requirement for 5G NR in FR2 (24 250 MHz–52 600 MHz).

BS class	Accuracy
Wide area BS	$\pm 0.05$ ppm
Medium range BS	$\pm 0.1$ ppm
Local area BS	$\pm 0.1$ ppm

obtain the  $T_b s^{-1}$  transmission rate, we believe that more efficient modulation formats will be used in the mm-wave or THz frequency band. Assuming that the mm-wave band uses 256 QAM and the THz band uses 64 QAM, the phase noise of the LO at mm-wave and THz band will be stricter. As a result, we can draw a general KPI for the 6G wireless communication system, as listed in table 7.

## 6.2. Describing performance requirements to the LO

**6.2.1. Requirement of frequency stability.** The modulated signal is up-converted (or down-converted) from the baseband to the RF band (or from RF to the baseband) in BS by mixing with the LO, as we discussed in section 1. The frequency stability of LO is the main factor that directly affects the frequency accuracy of the wireless network. The frequency shift of each NR carrier caused by the LO should be lower than the accuracy given in tables 7–9 observed over 1 ms. And the frequency shift  $f_s$  in ppm is calculated by dividing carrier frequency  $f_c$  into  $f_s$ ,

$$f_s(\text{ppm}) = \frac{10^6 \times f_s(\text{Hz})}{f_c}. \quad (9)$$

Based on this equation, we can analyze the criterion of frequency accuracy for a specific carrier. For example, if the

carrier frequency is 26 GHz, the frequency shift of the LO should be lower than 1.3 kHz observed over 1 ms.

**6.2.2. Requirement of phase noise.** The 31 dB SNR, the ADC quantization noise, the ADC clock jitter, and the phase noise of LO are the important effects resulting in the EVM of the wireless network [61, 105]. To evaluate the EVM caused by the phase noise, we need to analyze how the phase jitter results in the EVM. In the receiver, the QAM or QPSK signal is represented as an in-phase and quadrature message with respect to the carrier, which can be written as:

$$x(t) = m_I(t) \cos(\omega_{RF}t) + m_Q(t) \sin(\omega_{RF}t), \quad (10)$$

where  $m_I(t)$  and  $m_Q(t)$  represent the in-phase and quadrature amplitude,  $\omega_{RF}$  is the carrier frequency. In polar coordinates, the received signal can be written as:

$$x(t) = A(t) \cos(\omega_{RF}t + \phi(t)), \quad (11)$$

where  $A(t) = \sqrt{m_I^2(t) + m_Q^2(t)}$  and  $\phi(t) = \tan^{-1}(m_I(t)/m_Q(t))$  are the amplitude and the phase.

The received signal is mixed with the LO where a phase jitter  $\theta$  is added to  $\phi(t)$ . The mixed signal in in-phase and quadrature vector can be written as:

$$\begin{aligned} \vec{m}_I(t) &= 2A(t) \cos(\omega_{RF}t + \phi(t)) \cos(\omega_{LO}t + \theta) \\ &= A(t) \cos(\phi(t) - \theta) \end{aligned} \quad (12)$$

$$\begin{aligned} \vec{m}_Q(t) &= 2A(t) \cos(\omega_{RF}t + \phi(t)) \sin(\omega_{LO}t + \theta) \\ &= A(t) \sin(\phi(t) - \theta) \end{aligned} \quad (13)$$

where  $\omega_{LO}$  is the frequency of the LO. Here we assume that the receiver is homodyne,  $\omega_{LO} = \omega_{RF}$ . The constellation for received IF signal is expressed as:

$$\begin{aligned} S_{\text{real}} &= \vec{m}_I(t) + \vec{m}_Q(t) \\ &= A(t) [\cos(\phi(t) - \theta) + j \sin(\phi(t) - \theta)] \\ &= A(t) e^{j(\phi(t) - \theta)}. \end{aligned} \quad (14)$$

The real constellation minus the ideal constellation is the error of constellation, which can be written as:

$$\begin{aligned} S_{\text{error}} &= S_{\text{real}} - S_{\text{ideal}} = A(t) e^{j\phi(t)} (e^{-j\theta} - 1) \\ &= (\vec{m}_I + j\vec{m}_Q)(\cos \theta - 1 - j \sin \theta), \end{aligned} \quad (15)$$

where ideal constellation can be derived as  $S_{\text{ideal}} = A(t) [\cos \phi(t) + j \sin \phi(t)] = A(t) e^{j\phi(t)}$ . Furthermore, the error power caused by phase noise is expressed as:

$$\begin{aligned} P_{\text{error}} &= |S_{\text{error}}|^2 = \vec{m}_I(\cos \theta - 1) + \vec{m}_Q \sin \theta \\ &\quad + \vec{m}_Q(\cos \theta - 1) + \vec{m}_I \sin \theta \\ &= 2A^2(t)(1 - \cos \theta) \approx \theta^2 A^2(t). \end{aligned} \quad (16)$$

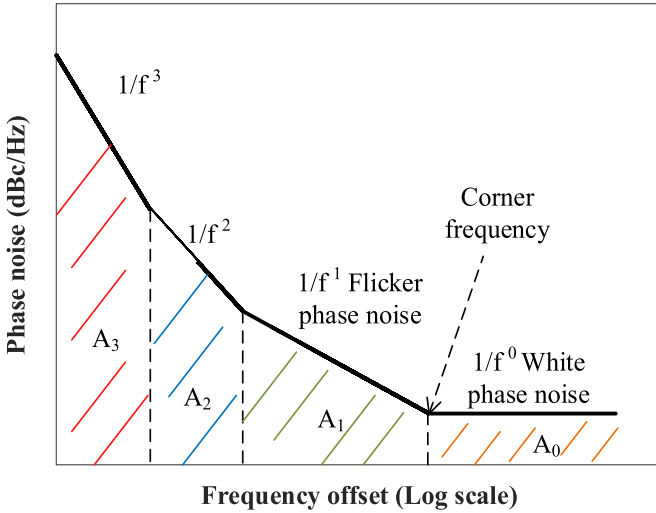


Figure 11. The customary characters of phase noise.

Therefore, the EVM caused by the phase noise is approximated to the phase jitter,

$$\text{EVM} = 100\% \times \sqrt{\frac{|S_{\text{error}}|^2}{|S_{\text{ref}}|^2}} = 100\% \times \sqrt{\frac{A^2(t)\theta^2}{A^2(t)}} = 100\% \times \theta(\text{rad}) \quad (17)$$

The phase jitter  $\theta$  of the LO is equal to the integration of phase noise power over the frequency range of interest, e.g. the area of the curve,  $A$ , as shown in figure 11. The lower bound of integration is set by the communication waveform time frame (generally 10–50 kHz), while the upper bound is set by the channel BW (100 or 800 MHz).

It is customary to characterize an oscillator in terms of its single-sideband phase noise as shown in figure 11. The actual curve of phase noise is approximated by several regions while each region has a slope of  $1/f^x$ . When  $x = 0$ , it corresponds to the ‘white’ phase noise region (slope = 0 dB dec<sup>-1</sup>), and  $x = 1$  corresponds to the ‘flicker’ phase noise region (slope = -20 dB dec<sup>-1</sup>).  $x = 2, 3, \dots$  are the offset frequencies close to the carrier frequency.

The individual power ratios are then summed and converted back into dB,

$$A = 10\log_{10}(A_0 + A_1 + A_2 + A_3). \quad (18)$$

Then the root-sum-square (RMS) phase jitter  $\theta$  in radians is given by the equation:

$$\theta(\text{rad}) = \sqrt{2 \times 10^{A/10}}. \quad (19)$$

Combining equations (17) and (19), the requirement of EVM in wireless networks is described by the requirement of the phase noise of the LO.

For different modulated formats, the EVMs caused by the phase noise is distinct. So, we take a 64 QAM waveform with the BW of 800 MHz as an example in the mm-wave band. Aforementioned, the RX system noise mainly consists of the 31 dB SNR, the ADC quantization noise, the ADC clock jitter, and the phase noise of LO. When the modulated format

is the 64 QAM, the total RX EVM is estimated as 4% and the part caused by phase noise is approximate 2.5% in the RX [61]. According to the equation (17), the phase jitter is equal to 0.025 rad and the power ratio is -32 dB, while the integration range is from 50 kHz to 800 MHz. In the RX system, we assume the corner offset frequency is 100 kHz, and the types of phase noise at 10 kHz and 1 MHz offset frequency are flicker and white phase noise, respectively. Then the power ratio of the phase noise is expressed as:

$$A = \text{PhaseNoise} + 10\log_{10}[800 \times 10^6 - 0.5 \times 10^6]. \quad (20)$$

If an EVM is lower than 2.5%, the phase noise of LO should be better than about -121 dBc Hz<sup>-1</sup> (at 1 MHz offset frequency) and -81 dBc Hz<sup>-1</sup> (at 10 kHz offset frequency), approximately. For the 64 QAM in mm-wave band, the state-of-art EIC oscillators and OEOs can meet the requirements of phase noise.

As we predict in the former sections, the indicator of EVM in the 6G era will be higher. The indicator of EVM is predicted as 3.5% for 256 QAM in mm-wave band and 8% for 64 QAM in THz band. Thus, the strict requirements pose a challenge for the LO and the LO with ultra-low phase noise is expected in the 6G era. Typically, we take the 256 QAM in the mm-wave band as an example. We assume the channel BW of mm-wave band in 6G is 800 MHz which is same as the mm-wave band in 5G, and the EVM due to the phase-noise jitter is estimated as 1% in the RX. According to the equation (17), the phase jitter is equal to 0.01 rad and the power ratio is -43 dB, while the integration range is from 50 kHz to 800 MHz. Then we can calculate the phase noise would be better than -132 dBc Hz<sup>-1</sup> (at 1 MHz offset frequency) and -92 dBc Hz<sup>-1</sup> (at 10 kHz offset frequency), if the EVM is lower than 1%. The requirement of phase noise may pose a challenge if the EIC oscillator serves as LO, but the OEO-based LO can easily reach the level of phase noise. Although the channel BW of THz band is not defined yet, it is foreseeable that the lower phase noise is needed to meet the requirements of THz communication in 6G.

## 7. LO distributed network: OEO based LO for 5G and beyond

5G communication system is being developed with several new scenarios, which include both evolution of today’s 4G networks and the globally standardized radio access technology known as NR. As we discussed in previous sections, higher carrier frequency, broader BW and more efficient modulated format for access networks are expected in 5G and beyond networks. Besides, network densification with crowded cells is generally expected to play an important role in 5G and beyond networks. So, distributing and synchronizing the LOs between a BBU pool and a series of RRUs are the key technologies in the fronthaul network. Thanks to the fiber-compatible architecture, OEO provides a potential solution.

In this section, we introduce the cloud, centralized, and co-operative radio access network (C-RAN) architecture in the 5G or 6G wireless network. Then an interconnected OEO technology is proposed to serve as the LOs network with the

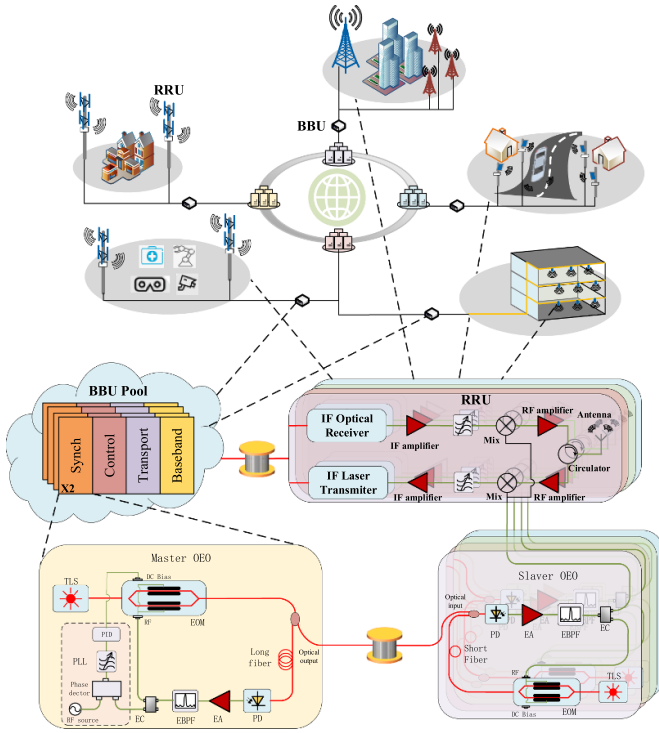


**Figure 12.** The scheme of the IL-OEO in wireless networks.

ultra-low-loss distribution and synchronization in the C-RAN. Furthermore, the requirements for the subsystem within the interconnected OEO architecture are analyzed and the feasible implementations for each part are also proposed to meet the new requirements of the LOs network in 5G and beyond.

### 7.1. C-RAN architecture for 5G and beyond network

To meet the new requirements of broadband and low-latency communication, the 5G technology introduces the mm-wave to carry a signal with a higher data rate. Subsequently, the size of a cell decrease to a few 10 m because of higher carrier frequency and higher data rate, which results in a denser BS, several access nodes (ANs) in a room. Also, the ANs mounted on a roadside lamp outdoors are necessary, as shown in figure 12.

In the access network of 5G communication, the C-RAN architecture is one of the essential technologies, and the BS is separated as BBU pool and RRUs in the C-RAN, as shown in figure 12. Such a separated architecture enables higher utilization, better energy efficiency and lower deployment costs because it shares the baseband resources between numerous radio cells. The BBU pool and RRUs are connected by a low-latency and high BW optical network. In the RRUs, the baseband signal is amplified, up-converted to the RF band by mixing with a LO and emitted by the antennas.

One of the challenges for C-RAN is the strict performance requirements of LO, including not only phase noise and frequency accuracy but also ultra-low-loss distribution and synchronization. IL-OEO seems an effective method to meet the

requirements, while the intrinsic characters of the optical networks enable the distribution and synchronization between BBU pool and RRUs. IL-OEO architecture between the BBU pool and RRUs is illustrated in figure 12. The requirements and feasible implementations of subsystems are introduced in the following.

### 7.2. Description of IL-OEO

Figure 12 shows the schematic illustration of IL-OEO. It consists of a high-performance master OEO in the BBU pool and a series of energy-efficient OEOs in RRUs. Connecting by low-latency and low-loss optical fronthaul networks, the mm-wave signal generated by master OEO is distributed to slave OEOs in RRUs. When the phases of two loops are locked by injecting a portion of the master-loop signal into the slave loop, the slave OEOs in RRUs are synchronized and achieve the low phase noises.

As we discussed in section 3, the theories and experimental demonstrations about IL-OEO have been developed in past years [69, 70, 75–77]. The IL-OEO achieves the ultra-low phase noises in both low- $Q$  oscillators and a high- $Q$  oscillator. In the former researches, the phase of the slave loop is locked to the phase of the master loop when the offset frequency is below to Leeson frequency. Beyond this frequency, the slave loop signal reaches a plateau, while the master loop's signal continuously decreases with the increasing offset frequency. Besides, the Leeson frequency blue shifts with the master-to-slave injection ratio, reducing the phase noise of the slave loop at high offset frequencies.

To meet the requirements of LOs in the 5G and beyond network, there are some specific considerations for the IL-OEO. For master OEO, ultra-low phase noise and high-frequency accuracy are expected. For slave OEO, energy efficiency, module size and deployment cost are primary requirements.

As we discuss in section 3, the phase noise is inversely proportional to the fiber length. Thus, a long fiber is necessary for the master OEO and some OEOs with low phase noise are reviewed in table 3. The frequency accuracy (or frequency stability) is another critical performance for master OEO. Because the fiber is sensitive to stress and temperature, the shift of oscillating frequency leads to deterioration of the long-term frequency stability. To solve this problem, several methods have been proposed and demonstrated, such as the temperature-insensitive fiber, the thermal stabilization and the PLL. Typically, Kaba *et al* replaced the standard SMF with a solid-core photonic crystal fiber (SC-PCF) to serve as an energy storage element for OEO and the frequency stability was improved to some extent [106]. However, such SC-PCF has high transmission loss, thereby increasing the power consumption. Thermal stabilization is another effective solution to relieve the negative influence of ambient environment variation. By using this method, Eliyahu *et al* proposed a high- $Q$  and stable OEO system [107]. In this proposal, the optical fiber and the narrow band-pass microwave filter are thermally stabilized by resistive heaters and temperature controllers. The frequency stability of free-running OEO is improved to



0.02 ppm under thermal stabilization, and the slope of frequency versus temperature improved from  $-8.3 \text{ ppm } ^\circ\text{C}^{-1}$  for non-thermally stabilized system to  $-0.1 \text{ ppm } ^\circ\text{C}^{-1}$ . By locking the OEO to a standard reference, it generates a 10 GHz signal with a phase noise of  $-143 \text{ dBc Hz}^{-1}$  at the 10 kHz offset frequency. Another effective solution is passively temperature stabilized OEO by using composite Hollow Core-Photonic Crystal Fiber (HC-PCF) and SMF-28 [108]. To cope with the power consumption of thermal stabilization, the thermal enclosure is also used to isolate the ambient environment variation. In [109], Zhang *et al* demonstrated that a single-loop OEO realizes a long-term frequency stability by using PLL technology. A high stable 3 GHz microwave signal is obtained by using this approach. The phase noise is  $-65 \text{ dBc Hz}^{-1}$  at 10 Hz offset frequency and the frequency stability is low to  $6.98 \times 10^{-14}$  for an average time of 1000 s.

On the other side, the slave OEO requires efficient-power consumption, small size and economical cost. However, the traditional OEOs have the demerits of bulky size and high power consumption. It is hard to meet the requirements of 5G and beyond network. Fortunately, with the development of the PIC, the integrated OEOs on several PIC platforms lead to a compact and easy-to-handle implementation, as we discussed in section 4. Since LO based on integrated OEO can greatly reduce the footprint and cost while considerably enhance the stability and energy efficiency, we believe it will make an outstanding contribution to the future wireless network.

### 7.3. Performances of IL-OEO for LOs network

In summary, a large number of LOs are required in the wireless network, because small-cell architecture and massive MIMO technology are massively used in the 5G and beyond network. Generating a microwave signal with high performances in a center BBU pool and distributing it to RRUs may arise a feasible option. Besides, synchronization, low power consumption and cost reduction are challenges for the LOs.

The fiber-compatible OEO system seems an effective method to meet the new requirements of LOs. For distributing and synchronizing the LOs in MIMO and CoMP technologies, the OEO has intrinsic superiority such as low latency, low loss and electromagnetic immunity. In this section, an IL-OEO architecture is implemented as the interconnect LOs network. In the IL-OEO-based LOs network, a master OEO in the center BBU pool generates a microwave signal with high performances, and then the signal is distributed to many slave OEOs in a series of RRUs. By using the IL-OEO technology, the slave OEO would be synchronized and their performances would be improved to the same level as master OEO. As we introduce in sections 3–6, the phase noise and frequency stability of OEO satisfy the new requirements of LO, while the characteristics of distribution and synchronization by using IL-OEO are suitable for the LOs network in 5G and beyond network. Besides, the PIC technologies provide a promising prospect to OEOs in power consumption and cost.

## 8. Conclusion

In this article, we discuss the prospect that OEOs serve as LOs in the 5G wireless network and beyond. Firstly, we review the developments of the EIC oscillators, discrete OEOs, and integrated OEOs, including the basic concept of operation and some milestones in the application. Secondly, we compare the performances of the EIC oscillator and the OEO in terms of the frequency stability, the phase noise, the power consumption, and the cost when they serve as a single-point LO. Thirdly, the criteria of LO are described according to the standard released by 3GPP. Lastly, an IL-OEO-based interconnect LO network is introduced to solve the distribution and synchronization within the C-RAN architecture of 5G and beyond wireless network.

In summary, the power consumption and cost of OEOs are much higher than EIC oscillators, but the OEO is better than EIC oscillators in the performance of phase noise at high frequency, which is greatly desired in the 5G wireless network and beyond. More importantly, thanks to the fiber-compatible architecture, IL-OEO-based LOs network seems an effective method to meet the requirements of distribution and synchronization of LOs in the 5G wireless network and beyond. With the development and industrialization of PIC, it is expected that the integrated OEO has a promising prospect in the future wireless network.

## Data availability statement

The data that support the findings of this study are available upon reasonable request from the authors.

## Acknowledgments

This work is supported in part by the NWO Zwaartekracht program on Integrated Nanophotonics; Open Fund of State Key Laboratory of Optoelectronic Materials and Technologies (Sun Yat-sen University); Key Research and Development Program of China (2018YFE0201000); The Zhejiang Provincial Natural Science Foundation of China (LQ20F010008); Sichuan Science and Technology Program (2020YFH0108); ZJU-TU/e IDEAS project. We acknowledge that the OEwaves, Inc. provides the permission to use the image of OE3710 HI-Q® Ka-BAND OEO. And we also thanks Prof. Daryoush from Drexel University provides some valuable advices for us to achieve better accuracy and clarity.

## ORCID iDs

Fang Zou  <https://orcid.org/0000-0002-9217-8249>

Bo Yang  <https://orcid.org/0000-0001-7837-3454>

Huiyun Liu  <https://orcid.org/0000-0002-7654-8553>

## References

- [1] Andrews J G, Buzzi S, Choi W, Hanly S V, Lozano A, Soong A C K and Zhang J C 2014 What will 5G be? *IEEE J. Sel. Areas Commun.* **32** 1065–82
- [2] Gupta A and Jha R K 2015 A survey of 5G network: architecture and emerging technologies *IEEE Access* **3** 1206–32
- [3] Lin J-C 2018 Synchronization requirements for 5G: an overview of standards and specifications for cellular networks *IEEE Veh. Technol. Mag.* **13** 91–99
- [4] Technical Specification Group Radio Access Network 3rd generation partnership project 2020–07 study on scenarios and requirements for next generation access technologies (release 16) *Document 3GPP TR 38.913 V16.0.0*
- [5] Technical Specification Group Radio Access Network 3rd generation partnership project 2020–06 NR, physical channels and modulation (release 16) *3GPP TS 38.211 V16.2.0*
- [6] Ziegler V and Yrjola S 2020 6G indicators of value and performance *2020 2nd 6G Wireless Summit (6G SUMMIT)* (IEEE) pp 1–5
- [7] Zong B, Fan C, Wang X, Duan X, Wang B and Wang J 2019 6G technologies: key drivers, core requirements, system architectures, and enabling technologies *IEEE Veh. Technol. Mag.* **14** 18–27
- [8] Stüber G L 2017 *Principles of Mobile Communication* (Berlin: Springer International Publishing)
- [9] Poddar A and Rohde U 2012 Latest technology, technological challenges, and market trends for frequency generating and timing devices *IEEE Microw. Mag.* **13** 120–34
- [10] Masoud B, Mina S and Robert B S 2019 *RF CMOS Oscillators for Modern Wireless Applications* (Copenhagen: River Publishers Series in Circuits and Systems)
- [11] Cao Z, Ma Q, Smolders A B, Jiao Y, Wale M J, Oh C W, Wu H and Koonen A M J 2015 Advanced integration techniques on broadband millimeter-wave beam steering for 5G wireless networks and beyond *IEEE J. Quantum. Electron.* **52** 0600620
- [12] Waterhouse R and Novack D 2015 Realizing 5G: microwave photonics for 5G mobile wireless systems *IEEE Microw. Mag.* **16** 84–92
- [13] Zou J, Sasu S A, Lawin M, Dochhan A, Elbers J-P and Eiselt M 2020 Advanced optical access technologies for next-generation (5G) mobile networks *J. Opt. Commun. Netw.* **12** D86
- [14] Ghosh A, Ratasuk R, Mondal B, Mangalvedhe N and Thomas T 2010 LTE-advanced: next-generation wireless broadband technology *IEEE Wirel. Commun.* **17** 10–22
- [15] Daryoush A 1990 Optical synchronization of millimeter-wave oscillators for distributed architecture *IEEE Trans. Microwave Theory Techn.* **38** 467–76
- [16] Daryoush A, Sato K, Horikawa K and Ogawa H 1997 Electrically injection-locked intermodal oscillation in a long optical cavity laser diode *IEEE Microw. Guid. Wave Lett.* **7** 194–6
- [17] Zou X, Liu X, Li W, Li P, Pan W, Yan L and Shao L 2015 Optoelectronic oscillators (OEOs) to sensing, measurement, and detection *IEEE J. Quantum. Electron.* **52** 0601116
- [18] Hao T, Tang J, Domenech D, Li W, Zhu N, Capmany J and Li M 2018 Toward monolithic integration of OEOs: from systems to chips *J. Lightwave Technol.* **36** 4565–82
- [19] Chembo Y, Brunner D, Jacquot M and Larger L 2019 Optoelectronic oscillators with time-delayed feedback *Rev. Mod. Phys.* **91** 035006
- [20] Hao T, Liu Y, Tang J, Cen Q, Li W, Zhu N, Dai Y, Capmany J, Yao J and Li M 2020 Recent advances in optoelectronic oscillators *Adv. Photonics* **2** 044001
- [21] Wikipedia Oscillation (available at: <https://en.wikipedia.org/wiki/oscillation>) (Accessed 23 July 2021)
- [22] Marion J B, Hornyak W F and French A P 1984 Post-use review: physics for science and engineering, part I *Am. J. Phys.* **52** 94
- [23] van der Pol B 1960 A theory of the amplitude of free and forced triode vibrations *Radio Rev. Sel. Sci. Pap.* **1** 754–62
- [24] van der Pol B 1934 The nonlinear theory of electric oscillations *Proc. Inst. Radio Eng.* **22** 1051–86
- [25] Ishihara O, Mori T, Sawano H and Nakatani M 1980 A highly stabilized GaAs FET oscillator using a dielectric resonator feedback circuit in 9–14 GHz *IEEE Trans. Microw. Theory Tech.* **28** 817–24
- [26] Esdale D J and Howes M J 1981 A reaction coefficient approach to the design of one port negative impedance oscillators *IEEE Trans. Microw. Theory Tech.* **29** 770–776
- [27] Siegman A E and Hagger H J 1964 Microwave solid-state masers *Electron. Power* **17** 65
- [28] Siegman A E 1986 *Lasers* (Mill Valley, CA: University Science Books)
- [29] Yao X S and Maleki L 1994 High frequency optical subcarrier generator *Electron. Lett.* **30** 1525–6
- [30] Wikipedia Electronic oscillator (available at: [https://en.wikipedia.org/wiki/Electronic\\_oscillator](https://en.wikipedia.org/wiki/Electronic_oscillator)) (Accessed 12 May 2021)
- [31] Thomson E 1893 Method of and means for producing alternating currents *US Pat.* **1** 630
- [32] Fleming J A 1919 *The Thermionic Valve and Its Developments in Radio-telegraphy and Telephony* (London: Wireless Press, Limited)
- [33] Hong S 2004 A history of the regeneration circuit: from invention to patent litigation *School of Biological Sciences and Program in the History and Philosophy of Science, Seoul National University, Seoul, Korea*
- [34] Armstrong E H 1915 Some recent developments in the audio receiver *Proc. Inst. Radio Eng.* **3** 215–38
- [35] Moore G 1965 Moore's law *Electron. Mag.* **38** 114
- [36] Brock D C and Moore G E 2006 *Understanding Moore's Law: Four Decades of Innovation* (Philadelphia: Chemical Heritage Foundation)
- [37] Chen G, Mukamel S, Beljonne D and Bredas J-L 1996 The coupled electronic oscillators vs the sum-over-states pictures for the optical response of octatetraene *J. Chem. Phys.* **104** 5406–14
- [38] Koepke M E and Hartley D M 1991 Experimental verification of periodic pulling in a nonlinear electronic oscillator *Phys. Rev. A* **44** 68–77
- [39] Rusin F S and Bogomolov G D 1969 Orotrotron—an electronic oscillator with an open resonator and reacting grating *Proc. IEEE* **57** 720–2
- [40] Vilches A, Navarro A, Asenjo R, Corbera F, Gran R and Garzarán M J 2016 Mapping streaming applications on commodity multi-CPU and GPU on-chip processors *IEEE Trans. Parallel Distrib. Syst.* **27** 1099–115
- [41] Zou X, Lu B, Pan W, Yan L, Stöhr A and Yao J 2016 Photonics for microwave measurements *Laser Photonics Rev.* **10** 711–34
- [42] Skolnik M I 1990 *Introduction to RADAR Systems* (New York: McGraw-Hill)
- [43] Pohl N, Jaeschke T and Aufinger K 2012 An ultra-wideband 80 GHz FMCW radar system using a sige bipolar transceiver chip stabilized by a fractional-N PLL synthesizer *IEEE Trans. Microw. Theory Tech.* **60** 757–65

- [44] Chagnard C, Gilbert P, Watkins A N, Beeler T and Paul D W 1996 An electronic oscillator with automatic gain control: EQCM applications *Sens. Actuators B* **32** 129–36
- [45] García-Martínez G *et al* 2011 Development of a mass sensitive quartz crystal microbalance (QCM)-based DNA biosensor using a 50 MHz electronic oscillator circuit *Sensors* **11** 7656–64
- [46] Schmitt R F, Allen J W and Wright R 2001 Rapid design of saw oscillator electronics for sensor applications *Sens. Actuators B* **76** 80–85
- [47] Pollet T, Van B M and Moeneclaey M 1995 Bit sensitivity of OFDM systems to carrier frequency offset and Wiener phase noise *IEEE Trans. Commun.* **43** 191–3
- [48] Meyr H 1998 Digital communication receivers: synchronization *Channel Estimation and Signal Processing* (New York: John Wiley and Son)
- [49] Tomba L 1998 On the effect of Wiener phase noise in OFDM systems *IEEE Trans. Commun.* **46** 580–3
- [50] Armada A G 2001 Understanding the effects of phase noise in orthogonal frequency division multiplexing (OFDM) *IEEE Trans. Broadcast.* **47** 153–9
- [51] Munier F, Alpman E, Eriksson T, Svensson A and Zirath H 2003 Estimation of phase noise for QPSK modulation over AWGN channels *Proc. GigaHertz 2003 Symp.* pp 4–5
- [52] Wu S and Bar-Ness Y 2004 OFDM systems in the presence of phase noise: consequences and solutions *IEEE Trans. Commun.* **52** 1988–96
- [53] Munier F, Eriksson T and Svensson A 2008 An ICI reduction scheme for OFDM system with phase noise over fading channels *IEEE Trans. Commun.* **56** 1119–26
- [54] Porret A-S, Melly T, Enz C C and Vittoz E A 2000 Design of high-Q varactors for low-power wireless applications using a standard CMOS process *IEEE J. Solid-State Circuits* **35** 337–45
- [55] Lee H, Choi T Y, Mohammadi S and Katehi L P B 2005 An extremely low power 2 GHz CMOS LC VCO for wireless communication applications *The European Conf. on Wireless Technology* (IEEE) pp 31–34
- [56] Quadrelli F, Panazzolo F, Tiebout M, Padovan F, Bassi M and Bevilacqua A 2019 A 18.2–29.3 GHz colpitts VCOs bank with  $-119.5$  dBc/Hz phase noise at 1 MHz offset for 5G communications *IEEE Radio Frequency Integrated Circuits Symp. (RFIC)* (Boston, MA, USA) pp 167–70
- [57] Hao G, Yong C, Mak P I and Rui P M 2019 A  $0.08\text{ mm}^2$  25.5-to-29.9 GHz multi-resonant-RLCM-tank VCO using a single-turn multi-tap inductor and CM-only capacitors achieving  $-191.6$  dBc/Hz FoM and 130 kHz  $1/f$  3 PN corner 2019 *IEEE Int. Solid-State Circuits Conf. (ISSCC)* (San Francisco, CA, USA) pp 410–2
- [58] Lightbody S, Shirazi A H M, Djahanshahi H, Zavari R and Shekhar S 2018 A  $-195$  dBc/Hz FoMT 20.8-to-28 GHz LC VCO with transformer-enhanced 30% tuning range in 65 nm CMOS *IEEE Radio Frequency Integrated Circuits Symp. (RFIC)* (Philadelphia, PA) pp 200–3
- [59] Yang Z, Yong C, Yang S, Mak P I and Martins R P 2019 16.8 A 25.4-to-29.5GHz 10.2mW Isolated Sub-Sampling PLL Achieving  $-252.9$  dB Jitter-Power FoM and  $-63$  dBc Reference Spur *IEEE Int. Solid-State Circuits Conf. (ISSCC)* (San Francisco, CA, USA) pp 270–2
- [60] Liao D, Zhang Y, Dai F F, Chen Z and Wang Y 2020 An mm-wave synthesizer with robust locking reference-sampling PLL and wide-range injection-locked VCO *IEEE J. Solid-State Circuits* **55** 1–11
- [61] Wagner E, Shana'a O and Rebeiz G M 2019 A very low phase-noise transformer coupled oscillator and PLL for 5G communications in  $0.12\text{ }\mu\text{m}$  SiGe BICMOS *IEEE Trans. Microw. Theory Tech.* **67** 1–13
- [62] Jalili H and Momeni O 2020 A 230 GHz high-power and wideband coupled standing wave VCO in 65 nm CMOS *IEEE J. Solid-State Circuits* **55** 547–56
- [63] Hao W, Chen J, Do J T S, Hooman R and Liu X 2018 High-efficiency millimeter-wave single-ended and differential fundamental oscillators in CMOS *IEEE J. Solid-State Circuits* **53** 2151–63
- [64] Khiyabani S, Khatibi H and Afshari E 2019 A compact 275 GHz harmonic vco with  $-2.6$  dBm output power in a 130 nm sige process 2019 *IEEE Custom Integrated Circuits Conf. (CICC)* (<https://doi.org/10.1109/CICC.2019.8780375>)
- [65] Yao X S and Maleki L 1996 Optoelectronic microwave oscillator *J. Opt. Soc. Am. B* **13** 1725–35
- [66] Levy E C, Horowitz M and Menyuk C R 2009 Modeling optoelectronic oscillators *J. Opt. Soc. Am. B* **26** 148–59
- [67] Chembo Y K, Larger L, Tavernier H, Bendoula R, Rubiola E and Colet P 2007 Instabilities of microwaves generated with optoelectronic oscillators *Opt. Lett.* **32** 2571–3
- [68] Yao X S, Maleki L, Yu J, Lutes G and Tu M 1998 Dual-loop opto-electronic oscillator *IEEE Int. Frequency Control Symp.* (<https://doi.org/10.1109/FREQ.1998.717952>)
- [69] Zhou W and Blasche G 2005 Injection-locked dual opto-electronic oscillator with ultra-low phase noise and ultra-low spurious level *IEEE Trans. Microw. Theory Tech.* **53** 929–33
- [70] Okusaga O, Adles E J, Levy E C, Zhou W, Carter G M, Menyuk C R and Horowitz M 2011 Spurious mode reduction in dual injection-locked optoelectronic oscillators *Opt. Express* **19** 5839–54
- [71] Peng H, Zhang C, Xie X, Sun T, Guo P, Zhu X, Zhu L, Hu W and Chen Z 2015 Tunable DC-60 GHz RF generation utilizing a dual-loop optoelectronic oscillator based on stimulated brillouin scattering *J. Lightwave Technol.* **33** 2707–15
- [72] Eliyahu D, Seidel D and Maleki L 2008 Phase noise of a high performance OEO and an ultra low noise floor cross-correlation microwave photonic homodyne system *IEEE Int. Frequency Control Symp. (Honolulu, HI)* pp 811–4
- [73] Dai J, Liu A, Liu J, Zhang T, Zhou Y, Yin F, Dai Y, Liu Y and Xu K 2017 Supermode noise suppression with mutual injection locking for coupled optoelectronic oscillator *Opt. Express* **25** 27060–6
- [74] Yao X S, Davis L and Maleki L 2000 Coupled optoelectronic oscillators for generating both RF signal and optical pulses *J. Lightwave Technol.* **18** 73–78
- [75] Zhang L, Poddar A K, Rohde U L and Daryoush A S 2017 Self-ILPLL using optical feedback for phase noise reduction in microwave oscillators *IEEE Photon. Technol. Lett.* **27** 624–7
- [76] Sun T, Zhang L, Poddar A K, Rohde U L and Daryoush A S 2017 Limits in timing jitters of forced microwave oscillator using optical self-ILPLL *IEEE Photon. Technol. Lett.* **29** 181–4
- [77] Sun T, Zhang L and Daryoush A S 2019 High-resolution X-band frequency synthesizer using SILPLL optoelectronic oscillators *IEEE Trans. Ultrason. Ferroelectr. Freq. Control* **67** 217–23
- [78] Li W and Yao J 2012 A wideband frequency tunable optoelectronic oscillator incorporating a tunable microwave photonic filter based on phase-modulation to intensity-modulation conversion using a phase-shifted fiber Bragg grating *IEEE Trans. Microw. Theory Tech.* **60** 1735–42
- [79] Yu Y *et al* 2020 Frequency stabilization of the tunable optoelectronic oscillator based on an ultra-high-Q



- microring resonator *IEEE J. Sel. Top. Quantum Electron.* **26** 8301009
- [80] Fan Z, Zhang W, Qiu Q and Yao J 2020 Hybrid frequency-tunable parity-time symmetric optoelectronic oscillator *J. Lightwave Technol.* **38** 2127–33
- [81] Peng H *et al* 2019 Ultra-low phase noise and frequency agile X-band frequency synthesizer based on a phase locked optoelectronic oscillator *2019 Joint Conf. IEEE Int. Frequency Control Symp. and European Frequency and Time Forum (EFTF/IFC) (Orlando, FL, USA)* pp 1–3
- [82] Chen G, Lu D, Guo L, Zhao W, Huang Y and Zhao L 2018 Frequency-tunable OEO using a DFB laser at period-one oscillations with optoelectronic feedback *IEEE Photonics Technol. Lett.* **30** 1593–6
- [83] Ly A, Auroux V, Khayatadeh R, Gutierrez N, Fernandez A and Llopis O 2018 Highly spectrally pure 90 GHz signal synthesis using a coupled optoelectronic oscillator *IEEE Photonics Technol. Lett.* **30** 1313–6
- [84] Zhu X, Jin T, Fu Y, Chi H, Zuo L, Liu W and Wang Q 2020 A frequency-stable optoelectronic oscillator based on passive phase compensation *IEEE Photonics Technol. Lett.* **32** 612–5
- [85] Yang B, Zhao H, Cao Z, Yang S, Zhai Y, Ou J and Chi H 2020 Active mode-locking optoelectronic oscillator *Opt. Express* **28** 33220–7
- [86] Hosseini S E, Banai A and Kärtner F X 2017 Tunable low-jitter low-drift spurious-free transposed-frequency optoelectronic oscillator *IEEE Trans. Microw. Theory Tech.* **65** 72625–35
- [87] Hasanuzzaman G K M, Iezekiel S and Kanno A 2020 W-band optoelectronic oscillator *IEEE Photonics Technol. Lett.* **32** 771–4
- [88] Zhang W and Yao J 2018 Silicon photonic integrated optoelectronic oscillator for frequency-tunable microwave generation *J. Lightwave Technol.* **36** 4655–63
- [89] Primiani P *et al* 2016 Tunable optoelectronic oscillator based on an integrated heterodyne source *IEEE Int. Topical Meeting on Microwave Photonics (MWP) (Long Beach, CA)* pp 251–4
- [90] Chen G, Lu D, Guo L, Deng Q, Zhao W and Zhao L 2017 An optoelectronic oscillator based on self-injection-locked monolithic integrated dual-mode amplified feedback laser *Asia Communications and Photonics Conf., OSA Technical Digest (Online)* (Optical Society of America) Su2A.10 (<https://doi.org/10.1364/ACPC.2017.Su2A.10>)
- [91] Zhang X, Zheng J, Pu T, Zhang Y, Shi Y, Li J, Li Y, Zhu H and Chen X 2019 Simple frequency-tunable optoelectronic oscillator using integrated multi-section distributed feedback semiconductor laser *Opt. Express* **27** 7036–46
- [92] Zou F *et al* 2021 Parity-time symmetric optoelectronic oscillator based on an integrated mode-locked laser *IEEE J. Quantum. Electron.* **57** 500209
- [93] Han J, Huang Y, Hao Y, Tang M, Wang F, Xiao J, Yang Y and Huang Y 2018 Wideband frequency-tunable optoelectronic oscillator with a directly modulated AlGaInAs/InP integrated twin-square microlaser *Opt. Express* **26** 31784–93
- [94] Srinivasan S, Spencer D T, Heck M J R, Norberg E, Fish G, Theogarajan L and Bowers J E 2013 Microwave generation using an integrated hybrid silicon mode-locked laser in a coupled optoelectronic oscillator configuration *CLEO: 2013, OSA Technical Digest (Online)* (Optical Society of America) CTu2G.2 ([https://doi.org/10.1364/CLEO\\_SI.2013.CTu2G.2](https://doi.org/10.1364/CLEO_SI.2013.CTu2G.2))
- [95] Volyanskiy K, Salzenstein P, Tavernier H, Pogurmirskiy M, Chembo Y K and Larger L 2010 Compact optoelectronic microwave oscillators using ultra-high Q whispering gallery mode disk-resonators and phase modulation *Opt. Express* **18** 22358–63
- [96] Li J, Lee H and Vahala K 2013 Microwave synthesizer using an on-chip Brillouin oscillator *Nat. Commun.* **4** 2097
- [97] Savchenkov A A *et al* 2010 Whispering-gallery mode based opto-electronic oscillators *IEEE Int. Frequency Control Symp. (Newport Beach, CA)* pp 554–7
- [98] Liao M, Huang Y, Weng H, Han J, Xiao Z, Xiao J and Yang Y 2017 Narrow-linewidth microwave generation by an optoelectronic oscillator with a directly modulated microsquare laser *Opt. Lett.* **42** 4251–4
- [99] Daryoush A S and Sun T 2018 Multi-mode lasers for self-forced opto-electronic oscillators in compact frequency synthesizers *IEEE J. Microw.* **1** 625–38
- [100] Tang J, Hao T, Li W, Domenech D, Baños R, Muñoz P, Zhu N, Capmany J and Li M 2018 Integrated optoelectronic oscillator *Opt. Express* **26** 12257–65
- [101] Maleki L 2011 Sources: the optoelectronic oscillator *Nat. Photon.* **5** 728–30
- [102] OEwaves Inc. OE3710 HI-Q® Ka-BAND OEO (Pasadena, CA, USA) (available at: <https://www.oewaves.com/oe3710>) (Accessed 24 July 2021)
- [103] Marpaung D, Yao J and Capmany J 2019 Integrated microwave photonics *Nat. Photon.* **13** 80–90
- [104] Zou X *et al* 2019 A multifunctional photonic integrated circuit for diverse microwave signal generation, transmission, and processing *Laser Photonics Rev.* **13** 1800240
- [105] Galton I and Wu C W 2019 Understanding phase error and jitter: definitions, implications, simulations, and measurement *IEEE Trans. Circuits Syst.* **1** 66 1–19
- [106] Kaba M, Li H-W, Daryoush A S, Vilcot J-P, Decoster D, Chazelas J, Bouwmans G, Quiquempois Y and Deborgies F 2008 Improving thermal stability of optoelectronic oscillators *IEEE Microw. Mag.* **7** 38–47
- [107] Eliyahu D, Sariri K, Taylor J and Maleki L 2003 Optoelectronic oscillator with improved phase noise and frequency stability *Proc. Int. Society for Optics and Photonics: Photonic Integrated Systems (San Jose, CA, USA)* vol 4998 pp 139–48
- [108] Zhang L *et al* 2013 Ultra low FM noise in passively temperature compensated microwave opto-electronic oscillators *IEEE MTT-S International Microwave and RF Conf. New Delhi, India 14-16 Dec. 2013* 1–4
- [109] Zhang Y, Hou D and Zhao J 2014 Long-term frequency stabilization of an optoelectronic oscillator using phase-locked loop *J. Lightwave Technol.* **32** 2408–14